# Quantifying the contribution of ocean advection and surface flux to the upper-ocean salinity variability resolved by climate model simulations

Lucas Cardoso Laurindo[1], Leo Siqueira[1], Justin Small[2], LuAnne Thompson[3], and Ben P. Kirtman[1]

[1]University of Miami
[2]National Center for Atmospheric Research (UCAR)
[3]University of Washington

September 30, 2023

## Abstract

This study examines the impact of ocean advection and surface freshwater flux on the non-seasonal, upper-ocean salinity variability in two climate model simulations with eddy-resolving and eddy-parameterized ocean components (HR and LR, respectively). We assess the realism of each simulation by comparing their sea surface salinity (SSS) variance with satellite and Argo float estimates. Our results show that, in the extratropics, the HR variance is about five times larger than that in LR and agrees with the Argo estimates. In turn, the extratropical satellite SSS variance is smaller than that from HR and Argo by about a factor of two, potentially reflecting the low sensitivity of radiometers to SSS in cold waters. Using a simplified salinity conservation equation for the upper-50-m ocean layer, we find that the advection-driven variance in HR is, on average, one order of magnitude larger than the surface flux-driven variance, reflecting the action of mesoscale processes.

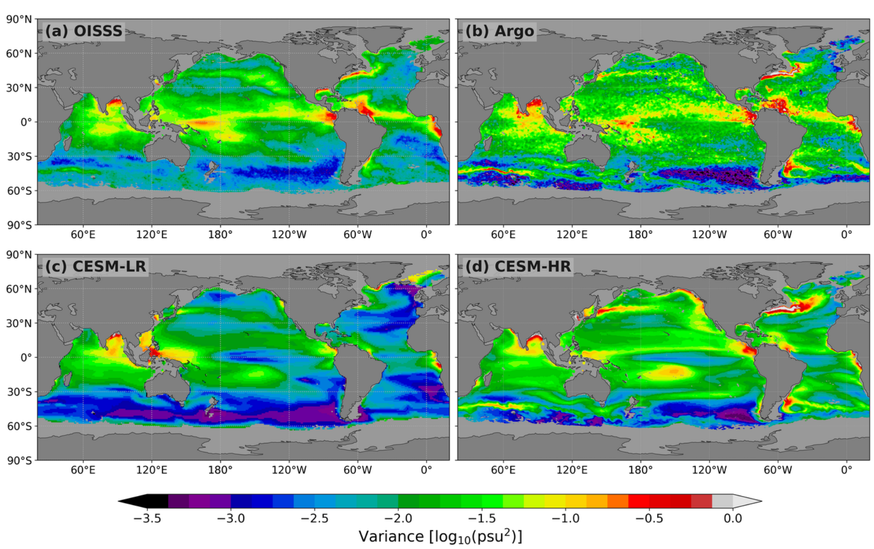

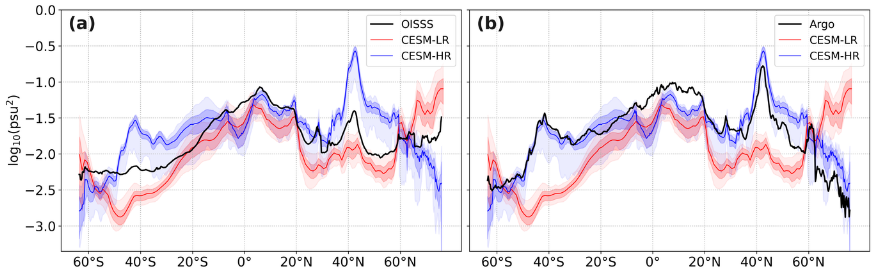
(a)
(b)
OISSS
Argo
CESM-LR
CESM-HR
$\log_{10}(\mathrm{psu}^2)$
0.0
−0.5
−1.0
−1.5
−2.0
−2.5
−3.0
60°S
40°S
20°S
0°
20°N
40°N
60°N

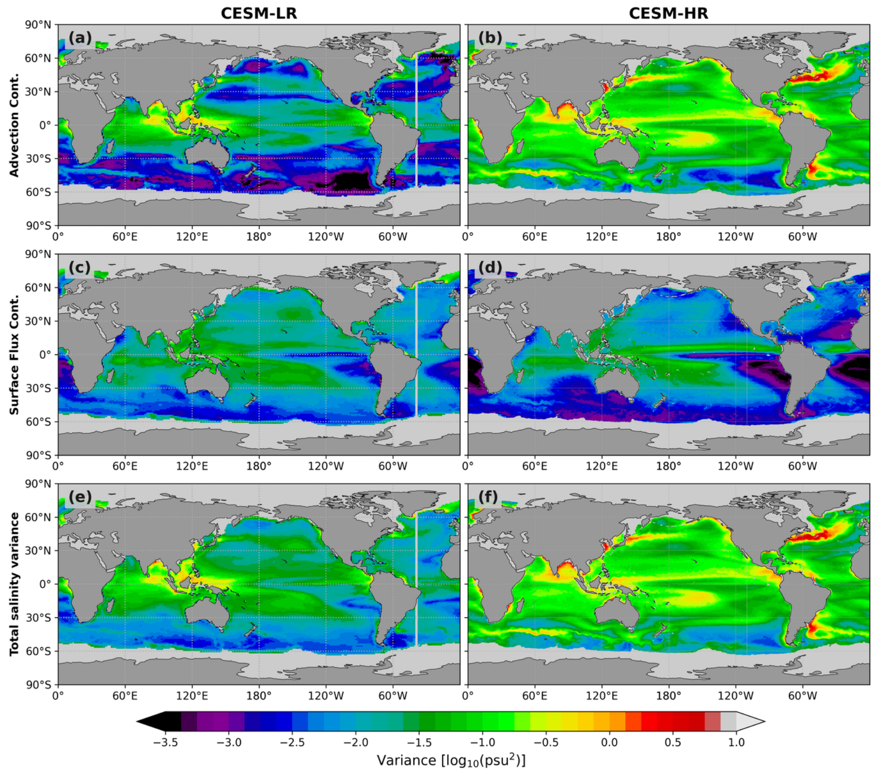
CESM-LR
CESM-HR
Advection Cont.
Surface Flux Cont.
Total salinity variance
(a)
(b)
(c)
(d)
(e)
(f)
90°N
60°N
30°N
0°
30°S
60°S
90°S
0°
60°E
120°E
180°
120°W
60°W
−3.5
−3.0
−2.5
−2.0
−1.5
−1.0
−0.5
0.0
0.5
1.0
Variance [$\log_{10}(\mathrm{psu}^2)$]

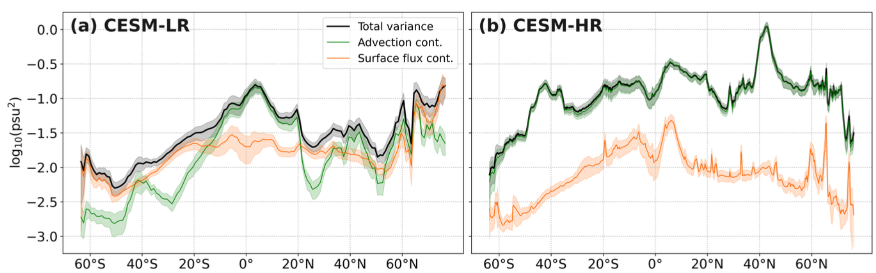
(a) CESM-LR
(b) CESM-HR
Total variance
Advection cont.
Surface flux cont.
$\log_{10}(\mathrm{psu}^2)$
0.0
−0.5
−1.0
−1.5
−2.0
−2.5
−3.0
60°S
40°S
20°S
0°
20°N
40°N
60°N

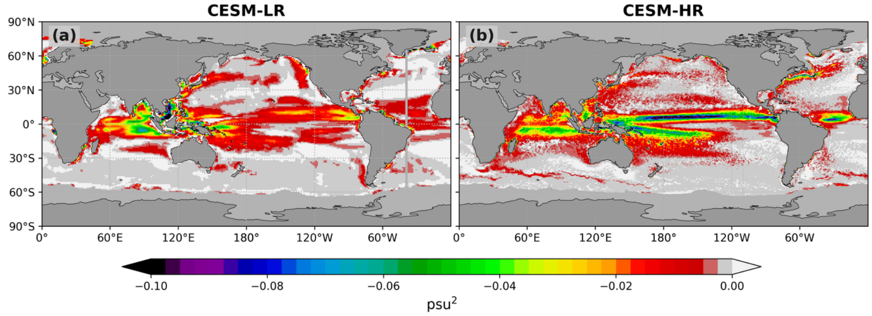
CESM-LR
CESM-HR
(a)
(b)
90°N
60°N
30°N
0°
30°S
60°S
90°S
0°
60°E
120°E
180°
120°W
60°W
−0.10
−0.08
−0.06
−0.04
−0.02
0.00
psu$^2$

# Quantifying the contribution of ocean advection and surface flux to the upper-ocean salinity variability resolved by climate model simulations

**Lucas C. Laurindo[1], Leo Siqueira[1,2], R. Justin Small[3], LuAnne Thompson[4], and Benjamin P. Kirtman[1,2,5]**

[1]Rosenstiel School of Marine, Atmospheric & Earth Science, University of Miami, Miami, FL, USA.
[2]Frost Institute for Data Science and Computing, University of Miami, Miami, FL, USA.
[3]Climate and Global Dynamics Laboratory, National Center for Atmospheric Research, Boulder, Colorado, CO, USA.
[4]School of Oceanography, University of Washington, Seattle, WA, USA.
[5]Cooperative Institute for Marine and Atmospheric Studies, University of Miami, Miami, FL, USA.

**Key Points:**

- We investigate how advection and surface flux affect upper-50-m salinity variance in eddy-resolving and eddy-parameterized climate models.
- The extratropical variance in the eddy-resolving run matches Argo and is much larger than in the eddy-parameterized run and satellite data.
- The larger upper-ocean salinity variance in the eddy-resolving run is predominantly driven by mesoscale ocean processes.

Corresponding author: Lucas C. Laurindo, `llaurindo@earth.miami.edu`

## Abstract

This study examines the impact of ocean advection and surface freshwater flux on the non-seasonal, upper-ocean salinity variability in two climate model simulations with eddy-resolving and eddy-parameterized ocean components (HR and LR, respectively). We assess the realism of each simulation by comparing their sea surface salinity (SSS) variance with satellite and Argo float estimates. Our results show that, in the extratropics, the HR variance is about five times larger than that in LR and agrees with the Argo estimates. In turn, the extratropical satellite SSS variance is smaller than that from HR and Argo by about a factor of two, potentially reflecting the low sensitivity of radiometers to SSS in cold waters. Using a simplified salinity conservation equation for the upper-50-m ocean layer, we find that the advection-driven variance in HR is, on average, one order of magnitude larger than the surface flux-driven variance, reflecting the action of mesoscale processes.



## Plain Language Summary

This study explores the importance of ocean currents, evaporation, and rainfall for driving changes in the salt concentration in the upper ocean (known as salinity) in two climate model simulations with differing ocean resolutions. The high-resolution model (HR) simulates ocean currents with dimensions of tens of km, while the low-resolution model (LR) can only simulate currents with hundreds of km in size. When comparing their simulated sea surface salinity variations with those captured by satellites and autonomous floats from the Argo array, the salinity variability in the high-resolution model is similar to the Argo data at mid to high latitudes and about five times stronger than that in the low-resolution model. The satellite data show a variability two times smaller than HR and Argo in the same regions, potentially due to low sensitivity to the surface salinity in cold waters. Using a simple equation describing the conservation of salinity in the upper ocean, we have shown that small-scale ocean currents drive most of the salinity variability in HR, while in LR, ocean currents play a much smaller role.


## 1 Introduction

Mesoscale ocean currents play a significant role in setting the upper-ocean temperature variability over much of the extratropical oceans. Indeed, estimates based on observations and model simulations indicate that the heat flux convergence associated with the mesoscale ocean eddy variability dominates over other terms of the heat budget equation at spatial scales smaller than about 1000 km and timescales ranging from intraseasonal to interannual (e.g., Putrasahan et al., 2017; Small et al., 2020; Martin et al., 2021;

Patrizio & Thompson, 2021, 2022) and potentially longer (Laurindo et al., 2022). While the conclusions drawn for the upper-ocean temperature suggest that advection by transient ocean motions can also be relevant for driving the upper-ocean salinity variability, only regional assessments of salinity have been made, and they show contrasting conclusions on the role of advection.

Results from the Salinity Processes in the Upper-ocean Regional Study (SPURS) field experiment conducted in the subtropical North Atlantic (SPURS-1, Lindstrom et al., 2015) indicate that the local time-averaged SSS is primarily balanced by the net surface fluxes acting to increase the salinity against the freshening effect of Ekman advection, seasonal fluctuations are mainly controlled by the seasonally-varying surface forcing, and interannual variations by surface fluxes and advection by Ekman currents, with little influence from mesoscale ocean processes (Dohan et al., 2015; Dong et al., 2015). In contrast, other studies show that freshwater advection by mesoscale ocean eddies contributes to the monthly to intraseasonal SSS variability in the region (Busecke et al., 2014; Centurioni et al., 2015; Farrar et al., 2015; Melnichenko et al., 2017), with model-based assessments also suggesting an important role in the time-averaged balance and on seasonal to interannual variations (Busecke et al., 2014; Gordon & Giulivi, 2014).

Treguier et al. (2012) showed that mesoscale eddies are essential for balancing the meridional freshwater transport in an eddy-resolving, 1/12° horizontal resolution ocean simulation of the North Atlantic, a mechanism that was absent in a corresponding eddy-permitting, 1/4° resolution run. The eddy-induced freshwater transport inferred by Treguier et al. (2012) was consistent with satellite and hydrography-based estimates for the region (Stammer, 1998; Amores et al., 2017; Melnichenko et al., 2017). Model results also indicate that eddy stirring enhances horizontal salinity gradients where small-scale mixing can occur (Bryan & Bachman, 2015).

In the eastern equatorial North Pacific, results from a second SPURS experiment (SPURS-2, Lindstrom et al., 2019) indicate that the local upper-ocean salinity budget is predominantly balanced by the freshening effect of the surface fluxes and the salting induced by vertical advection, with monthly to seasonal variations in the region driven by fluctuations in the Ekman advection (Farrar & Plueddemann, 2019; Melnichenko et al., 2019). In addition, satellite data indicates that westward propagating eddies contribute to the intraseasonal SSS variability in the area and that interannual changes reflect variations in the surface freshwater fluxes associated with the El Niño-Southern Oscillation (ENSO) cycle (Melnichenko et al., 2019).

The differing conclusions on the importance of mesoscale ocean currents for driving the SSS variability may stem from uncertainties of the observational datasets used, the geographical locations and size of the control volumes used, and the different temporal averaging periods used in the assessments (Lindstrom et al., 2015). The configuration of model experiments may have contributed to the divergence in the literature, as the horizontal ocean resolution controls the mesoscale current variability and the associated tracer transport (Kirtman et al., 2012; Treguier et al., 2012; Small et al., 2014; Chang et al., 2020). Further, most previous modeling studies used ocean-only simulations that cannot account for coupled ocean-atmosphere feedbacks on surface freshwater flux (e.g., Frenger et al., 2013; Light et al., 2022), and that rely on physically unrealistic sea surface salinity restoring schemes (Spall, 1993; Kamenkovich & Sarachik, 2004; Q. Zhang et al., 2022).

Here, we examine the influence of mesoscale processes on the monthly upper-ocean salinity variance at global scales from two fully coupled climate model simulations configured with eddy-resolving and eddy-parameterized ocean components. We quantify the contribution of ocean advection and surface freshwater fluxes to the upper-ocean salinity variability resolved by each simulation using saved terms in the salinity budget and assess their realism by comparing their global sea surface salinity (SSS) variance maps with that estimated using satellite and Argo float data.

Our work is organized as follows. Section 2 describes the observational products and climate model simulations (2.1), the methods applied for computing the upper-ocean salinity variance from the datasets used (2.2), and the budget equation used to decompose the model salinity variance into advection-driven and surface flux driven components (2.3). The results are presented and discussed in Section 3, while Section 4 summarizes this study and its conclusions.

# 2 Methods

## 2.1 Data description

### *2.1.1 Satellite sea surface salinity data*

We use near-global satellite SSS data for September 2011 to March 2022 from the Multi-Mission Optimally Interpolated Sea Surface Salinity dataset (OISSS, Melnichenko et al., 2016, 2021). This product combines observations from three satellites: Aquarius/ SAC-D (August 2011 to June 2015), Soil Moisture Active Passive (SMAP, March 2015 until the present), and Soil Moisture and Ocean Salinity (SMOS, January 2010 to present). Their primary instruments are passive microwave radiometers that measure the surface radiative flux along wide ground swaths. The measurements are taken in the L-band radiometric frequency band ($\sim$1.4 GHz), where the equivalent surface brightness temperature is highly correlated with SSS for sea surface temperatures above 5°C (Klein & Swift, 1977). However, these correlations rapidly drop for temperatures less than 5°C (Meissner et al., 2018; Dinnat et al., 2019; Vinogradova et al., 2019). The OISSS data is produced at a $0.25° \times 0.25° \times 4$-day grid, has a 0.19 psu root mean square difference relative to *in situ* measurements, and near-zero bias.

#### *2.1.2 Vertical salinity profiles from Argo floats*

We utilize about two and a half million quality-controlled vertical salinity profiles obtained from January 1998 to December 2020 by Argo profiling floats (Good et al., 2013; Wong et al., 2020). The Argo floats are designed to drift in neutral equilibrium at 1000 or 2000 m depth, emerging every ten days to measure pressure, temperature, and salinity as they rise. After transmitting their position and data to land-based receiving stations, the floats return to their drifting depth until the next sampling cycle. The Argo array is globally distributed and currently has more than 3800 floats that gather about 12,000 profiles each month.

#### *2.1.3 CESM climate model outputs*

We analyze two climate simulations produced using the Community Earth System Model version 1.3 (CESM, Meehl et al., 2019; S. Zhang et al., 2020) with differing horizontal resolutions in the ocean and atmosphere. The first is low-resolution (LR), using a nominal 1° resolution in both components that requires parameterizing the effects of mesoscale ocean processes (e.g., Gent & McWilliams, 1990). The second is high-resolution (HR), using a 0.25° resolution in the atmosphere and 0.1° in the ocean that is eddy-resolving except at high latitudes. LR is integrated for 501 years and HR for 519 years, both using 1850 $CO_2$ forcing. These simulations are thoroughly described in Chang et al. (2020).

The CESM outputs used in this work are monthly-averaged horizontal fields of SSS and surface freshwater flux, and three-dimensional monthly global fields of ocean salt flux convergence computed using horizontal and vertical advection components. The LR (HR) quantities are obtained for the simulation years 1–249 (338–519), following their availability in the model output files.

### 2.2 Estimating the salinity variance using observations and CESM data

To compute variance maps, we define salinity anomalies as fluctuations about a best-fit model composed of the long-term mean, a linear temporal trend, and of annual and semiannual harmonics representing the seasonal cycle. We first compute monthly averages of the 4-day resolution satellite SSS data for consistency with the model outputs before isolating the monthly anomalies. In turn, using model data, we estimate the SSS variance for 10-year segments of the monthly outputs to simulate the length of the satellite record. This results in twenty-one global SSS variance maps for LR and eighteen for HR, which we use to estimate the uncertainty of the SSS variance levels resolved by the simulations.

In the case of the Argo vertical salinity profiles, SSS data is unavailable as the shallowest measurements are taken at 5-m depth or more. Thus, we consider the average salinity measured by the floats over the first 10 m of the water column as a proxy for SSS, consistent with the 10-m thickness of the CESM surface ocean layer. We also low-pass filter the 10-day resolution data along the float trajectories at thirty days to reproduce the monthly sampling frequency of the model data. Finally, we use the data binning procedure described in Laurindo et al. (2017) to decompose the Argo measurements into time-mean, seasonal, and eddy components, the latter of which are used to compute a regular-gridded ($0.25° \times 0.25°$ resolution) global salinity variance map.

### 2.3 Decomposing the CESM upper-ocean salinity variance

Inspired by the analysis of Patrizio and Thompson (2021), here we use a simplified salinity conservation equation to diagnose the contribution of the ocean advection and surface freshwater fluxes to the monthly salinity variability in a surface layer of thickness $h = 50$-m resolved by the HR and LR simulations, given by:

$$\frac{\partial \langle S \rangle}{\partial t} = \underbrace{-\langle \nabla \cdot (\mathbf{u} S) \rangle}_{\text{Ocean advection } (Q_o)} + \underbrace{\frac{S_0}{h}(E - P)}_{\text{Surface fluxes } (Q_s)} , \tag{1}$$

where the brackets denote quantities vertically averaged over the upper 50-m, $\mathbf{u}$ is the three-dimensional velocity vector, $S$ represents salinity, $E$ evaporation, $P$ precipitation, and $S_0$ is a constant reference salinity equal to 34.7 psu. The first term on the right-hand side represents the salt flux convergence associated with the three-dimensional ocean advection ($Q_o$), and the second term the surface freshwater flux ($Q_s$). Eq. (1) omits the contributions of entrainment at the bottom of the layer and of diffusive processes.

Dropping the brackets for simplicity and isolating monthly mean anomalies (represented by primes) from (1) yields:

$$\frac{\partial S'}{\partial t} = Q'_o + Q'_s, \tag{2}$$

from which we obtain an analytical expression for the salinity variance $\sigma_S^2$ by centered differencing the salinity tendency term, squaring both sides of the equation, and taking a time average:

$$\sigma_S^2 = \frac{2\Delta t^2}{1 - r_2}\left(\overline{Q_o'^2} + \overline{Q_s'^2} + 2\overline{Q'_o Q'_s}\right), \tag{3}$$

where $\Delta t$ represents the sampling interval of one month, and $r_2$ is the two-month lag autocorrelation of the vertically-averaged salinity (Patrizio & Thompson, 2021).

From (3), we define the diagnostic relationship:

$$\sigma_S^2 = \tilde{Q}_{oo} + \tilde{Q}_{ss} + \tilde{Q}_{os}, \tag{4}$$

where $\tilde{Q}_{oo}$ and $\tilde{Q}_{ss}$ represent the contribution of ocean advection and surface freshwater flux for driving the upper-ocean salinity variability, respectively, while $\tilde{Q}_{os}$ arises from the covariance between advection and surface fluxes. They are expressed as:

$$\tilde{Q}_{oo} = \frac{2\Delta t^2}{1 - r_2}\overline{Q_o'^2}, \tag{5}$$

$$\tilde{Q}_{ss} = \frac{2\Delta t^2}{1 - r_2}\overline{Q_s'^2}, \tag{6}$$

$$\tilde{Q}_{os} = \frac{4\Delta t^2}{1 - r_2}\overline{Q'_o Q'_s}. \tag{7}$$

We use (4) to (7), combined with the salt flux convergence and surface freshwater flux outputs, to estimate $\sigma_S^2$, $\tilde{Q}_{oo}$, $\tilde{Q}_{ss}$, and $\tilde{Q}_{os}$ for HR and LR. We note that the CESM budget outputs are for the conservation of salt content rather than of salinity. While both are equivalent at subsurface layers, undulations of the free surface can strongly modulate the salt content of the surface layer but not its salinity (c.f. Sec. 3.3 of Smith et al., 2010). Since we focus on the salinity variability, here we examine advection outputs vertically-averaged over the 10 to 50 m layer as a proxy for the upper-50-m salinity flux convergence $Q_o$. We isolate the monthly anomalies $Q'_o$ and $Q'_s$ using the methods described in Sec. 2.2, which are then applied in Eqs. (4) to (7) for computing the quantities of interest.

# 3 Results and discussion

## 3.1 Salinity variance in observations and CESM simulations

Here, we compare the non-seasonal, monthly SSS variance calculated using OISSS data, Argo data, and outputs from LR and HR. The large-scale patterns observed in the OISSS data (Fig. 1a) resemble those of the long-term mean precipitation (e.g., Adler et al., 2003; Xie et al., 2017), with enhanced values found in the vicinity of the Intertropical Convergence Zone (ITCZ) in the Atlantic and Pacific basins and over much of the Indian Ocean. This may indicate the influence of transient precipitation events from small-scale convective systems. The enhanced SSS variance within the tropics can also be attributed to advection by Ekman currents and Tropical Instability Waves (Melnichenko et al., 2019). In addition, significant SSS variances are associated with the freshwater discharge of major rivers, such as the Amazon (Congo) in the western (eastern) tropical Atlantic, the La Plata in the western South Atlantic, the Mississippi in the Gulf of Mexico, and the Ganges in the Bay of Bengal (Fournier & Lee, 2021). Moving to the extratropics, enhanced SSS variance appears in strong current systems, most prominently the Gulf Stream seaward extension, and to a lesser degree in the Kuroshio Current, Brazil Current, the Brazil-Malvinas Confluence, and the Agulhas Current System. The large SSS variance in these regions coincides with strong time-mean horizontal SSS gradients, suggesting that it arises from horizontal advection by mesoscale ocean currents (Amores et al., 2017; Melnichenko et al., 2017, 2019).

The upper-10-m salinity variance from Argo (Fig. 1b) show similar spatial distribution and magnitudes within the tropics. However, the Argo estimates resolve spatial patterns associated with all major extratropical current systems that are better defined and with larger magnitudes. In particular, the Argo estimates show values of up to 1.8 psu$^2$ (whose logarithm is $\sim 0.2$, for visualization in Fig. 1) at the Gulf Stream seaward extension, compared to only 0.3 psu$^2$ in OISSS (log $\sim -0.7$). About one order of magnitude differences are also seen at the Brazil-Malvinas Confluence and the Kuroshio and Agulhas Currents. The Argo estimates further show enhanced variances associated with the Antarctic Circumpolar Current (ACC) that are absent in OISSS. Also absent are zonally-elongated variance bands of about 0.03 psu$^2$ (log $-1.5$) south of Australia and in the Pacific and Atlantic subtropical gyres. Finally, Argo prominently show wide low variance regions ($\leq$0.01 psu$^2$, or $\leq -2$ in log scale) in the Southern Ocean that coincides with low eddy kinetic energy regions (Lumpkin & Johnson, 2013).

The comparison between the LR and HR variances provides further insight into the importance of mesoscale processes. Similarly to observations (Figs. 1a-b), HR re-

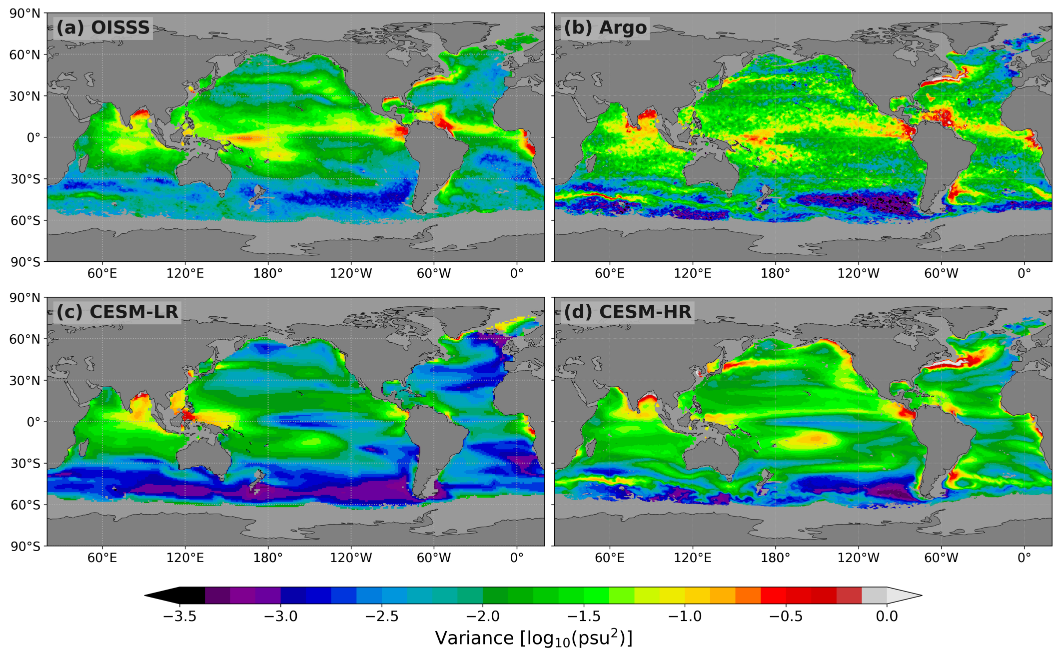


**Figure 1.** Monthly sea surface salinity (SSS) variance resolved by the OISSS satellite product (a), of the upper-10-m averaged salinity estimated using from Argo float data (b), and of the monthly SSS variance resolved by the low- and high-resolution CESM simulations (c and d). All estimates are shown in logarithmic scale.

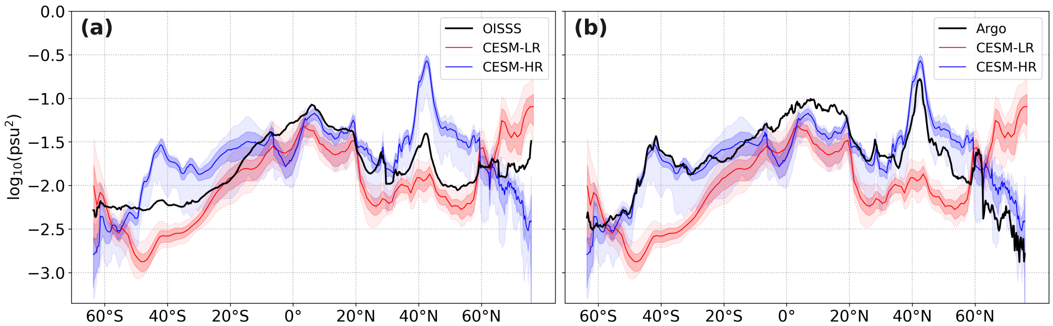


**Figure 2.** Zonally-averaged SSS variance from low- and high-resolution CESM simulations (red and blue lines, respectively), contrasted against zonally-averaged observational estimates (black lines) of the SSS variance resolved by the OISSS satellite product (panel a) and the upper-10-m salinity variance computed using Argo data (b). The darker shading around the CESM estimates is the standard deviation of the zonally-averaged salinity variances of individual ten-year segments of the model outputs, while the lighter shading show the minimum and maximum values obtained over all segments. All estimates are shown in logarithmic scale.

solves the enhanced variability associated with extratropical current systems, features absent in the LR results (Figs. 1c-d). Notably, the spatial features and variance levels resolved by HR in the extratropics resemble those shown by the Argo results.

Zonally-averaged salinity variances (Fig. 2) reinforce the similarity between the HR and Argo results in the extratropics and that both are significantly larger than those from LR. The zonally-averaged variance estimates from Argo (Fig. 2b) fall within one standard deviation of the ensemble-averaged HR variance estimates (computed as described in Sec. 2.2) in the Southern Hemisphere, and are generally larger than the minimum variance for HR in the Northern. In turn, the variance from OISSS (Fig. 2a), albeit larger than those from LR at most latitudes, are muted relative to Argo and HR between about 60°S and 55°N and exceed the variance levels resolved by both Argo and HR poleward of these latitudes. These characteristics likely reflect the smaller sensitivity of the SSS satellite retrievals in cold waters (Klein & Swift, 1977; Meissner et al., 2018; Dinnat et al., 2019; Vinogradova et al., 2019). Further highlighting the similarity between HR and Argo and their larger variance levels relative to LR and OISSS, the global area-averaged SSS variances are 0.009, 0.018, 0.021, 0.014 psu$^2$ for LR, HR, Argo, and OISSS respectively. Considering only latitudes poleward of 23°, these values change to 0.002, 0.010, 0.011, and 0.004 psu$^2$ for LR, HR, Argo, and OISSS, respectively.

Despite the higher overall realism of HR relative to LR, there are important differences relative to observations. In particular, OISSS and Argo both show larger and spatially more widespread salinity variance off the mouth of large rivers than HR, most prominently for the Amazon and Congo, potentially reflecting issues with the river runoff scheme in CESM-HR. Observations also show local salinity variance maxima in the western tropical Pacific, associated with the Indo-Pacific Warm Pool (De Deckker, 2016), that are imperfectly reproduced in HR. Specifically, the HR shows high variance values over the equator that are shifted west and closer to Indonesia relative to that from OISSS and Argo, while the high variances centered at about 10°S are shifted east by almost thirty degrees. These biases can be associated with deficiencies in how CESM represents atmospheric phenomena within the tropics, such as Madden-Julian Oscillations, tropical cyclones, and the ITCZ, as documented in Chang et al. (2020).

### 3.2 Role of advection and surface flux in the CESM salinity variance

In this Section, we examine the contribution of ocean advection and surface freshwater fluxes to the upper-50-m salinity variance, as resolved by HR and LR simulations, using Eqs. (4) to (7). The advection-induced salinity variance [$\tilde{Q}_{oo}$, Eq. (5)] is much higher in HR than in LR, except in the Indo-Pacific Warm Pool and in the eastern tropical Pacific, where both simulations show comparable values (Figs. 3a-b). The contribution of surface freshwater fluxes [$\tilde{Q}_{ss}$, Eq. (6)] is similar in both simulations, except in the Southern Ocean and in the western portion of the oceanic basins, where it can be up to one order of magnitude larger in LR relative to HR (Figs. 3c-d). The spatial distribution of the surface flux-induced variance is similar to climatological precipitation (e.g., Adler et al., 2003; Xie et al., 2017). The contribution of the covariance between advection and surface fluxes to the total salinity variance [$\tilde{Q}_{os}$, Eq. (7)] is smaller in magnitude than the other two components and shows predominantly negative values, whose spatial distribution mirrors that of the surface fluxes (Fig. S1). The global area-averaged values of the advection, surface flux, and covariance components are 0.019, 0.010, and $-0.003$ psu$^2$ for LR, in contrast to 0.092, 0.007, and $-0.005$ psu$^2$ for HR.

The sum of all components [$\sigma_S^2$, Eq. (4), Figs. 3e-f] produce salinity variance fields for LR and HR with spatial features similar to the respective monthly SSS variance fields (Figs. 3c-d), although with larger magnitudes, especially for HR. This is because $\sigma_S^2$ is obtained from monthly-averaged outputs of advection and surface freshwater flux, which are components of the salinity tendency that result from the difference between the instantaneous salinity from the beginning and end of each simulation month, while the SSS variances are computed using monthly-averaged salinity outputs that attenuate high-frequency

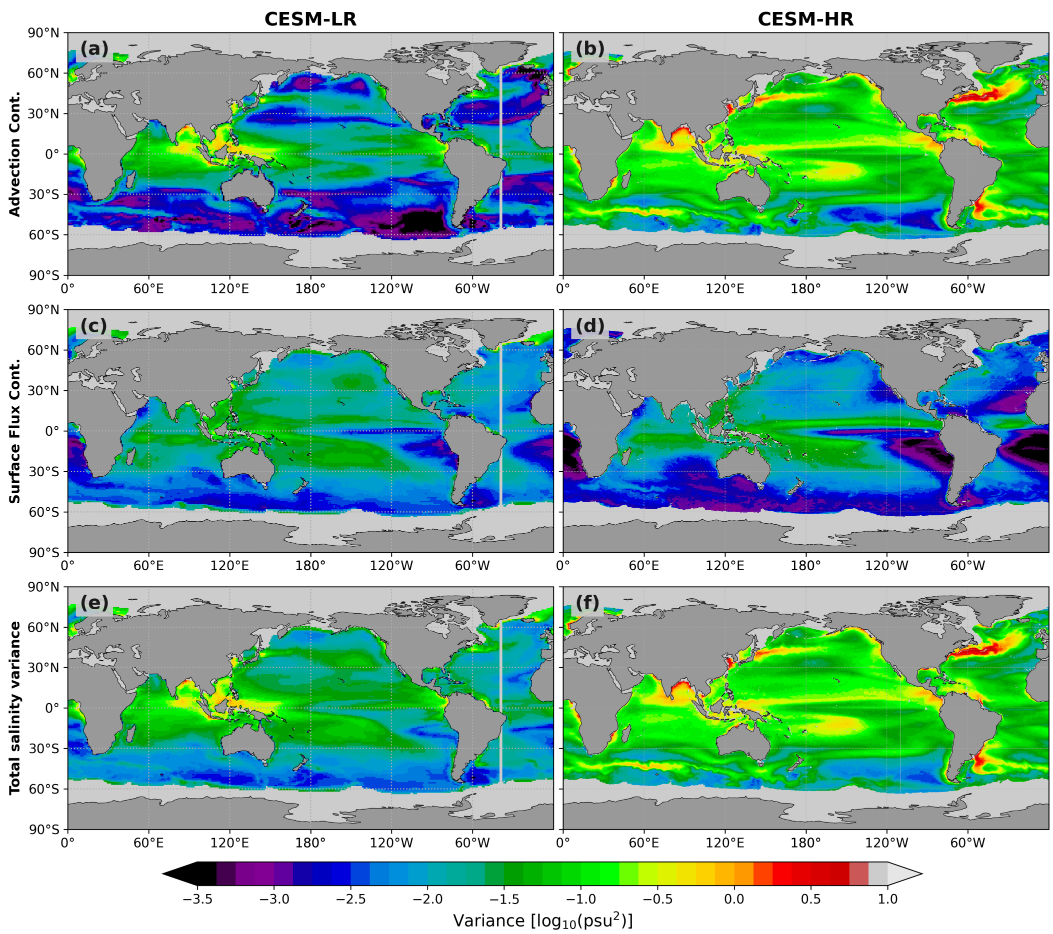


**Figure 3.** Contribution of ocean advection (a, b) and of surface freshwater fluxes (c, d) to the upper-50 m salinity variance (e, f) resolved by the low- and high-resolution CESM simulations. All estimates are shown in logarithmic scale.

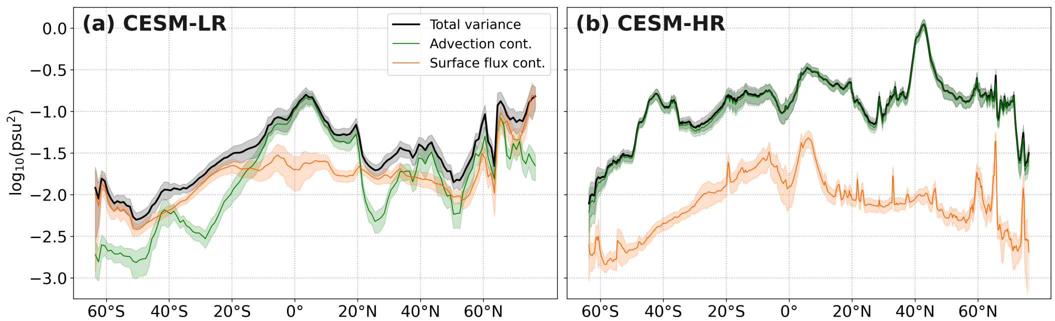


**Figure 4.** Zonally-averaged contributions of ocean advection and surface freshwater flux (orange and green lines, respectively) to the total salinity variance (black lines) for the low- and high-resolution CESM simulations (panels a and b, respectively). The shading around the estimates are the standard deviation of the zonally-averaged variances computed for individual ten-year segments of the model outputs. Estimates are shown in logarithmic scale.

variability. Here, the global area-average variances and 0.026 psu$^2$ for LR and 0.094 psu$^2$ for HR, about three and five times larger, respectively, than the corresponding values obtained for SSS.

Specifically in LR, the upper-ocean salinity variance is dominated by advection within the tropics and at western boundary currents, and by surface fluxes in the Southern Ocean and at the interior of all subtropical gyres (Fig. 3). Zonal averages of the advection- and surface-flux-induced salinity variance further highlights that surface fluxes predominantly drive the variance south of 20°S while north of 20°N both components contribute about equally (Fig. 4). In turn, the HR salinity variance is dominated by advection virtually everywhere, with a contribution from the surface fluxes only noticeable at quiescent, low salinity variance regions in the Southern Ocean (Figs. 3 and 4).

These results show that the larger upper-ocean salinity variance levels in HR are due to larger advective flux variability compared to LR. The advective fluxes consist of Ekman and geostrophic components, with the Ekman dynamics being forced by the atmosphere via wind stress and contributing to the SST variability within the tropics (Larson et al., 2018; Small et al., 2020). Geostrophic current variability near the equator is explained by large-scale, equatorially-trapped waves such as Rossby and Tropical Instability Waves, while in the extratropics it is explained by mesoscale eddies (Tulloch et al., 2009; Chelton et al., 2011), which dominate the non-seasonal SST variability in eddy-resolving simulations (Delworth et al., 2012; Kirtman et al., 2012; Putrasahan et al., 2017; Small et al., 2020; Laurindo et al., 2022).

We note that the simulations also have different horizontal atmospheric resolutions (0.25° vs. 1°), which enables a more accurate representation of phenomena such as weather fronts and tropical cyclones in HR. These phenomena significantly affect precipitation (Chang et al., 2020; Light et al., 2022) and likely also impact the upper-ocean salinity variance. The outline of the ITCZ in the tropical Pacific, seen in all variance components calculated using HR data [Eq. (4) and Figs. 3 and S1], is a potential signature of the influence of resolved atmospheric phenomena. This feature is weaker in LR. Previous studies have demonstrated that the influence of intrinsic ocean and atmosphere phenomena on upper-ocean temperature can be distinguished by the spatial and temporal scales where they operate (Small et al., 2019, 2020; Laurindo et al., 2019, 2022). Future studies can potentially apply similar methods to disentangle the influence of atmospheric and oceanic processes in the upper-ocean salinity variability.

## 4 Summary and conclusions

In this study, we use a simplified salinity conservation equation to quantify the contribution of ocean advection and surface freshwater flux to the non-seasonal, upper-50-m ocean salinity variability resolved by century-long CESM simulations configured with eddy-resolving and eddy-parameterized ocean resolutions (HR and LR, respectively). We determine the overall realism of each model run by contrasting their SSS variance with those calculated using ten years of satellite SSS data from the OISSS product and twenty-one years of upper-10-m averaged salinity data from Argo floats.

We find that the upper-ocean salinity variance in HR is, on average, twice as large as that from LR. The difference increases to a factor of five if we only consider the extratropics. The most significant differences occur in western boundary current systems and the ACC, where the variance can be one order of magnitude larger in HR. Relative to observations, the variance level resolved by HR is in excellent agreement in the extratropics with that estimated using Argo data and is two times larger than the OISSS satellite estimates. OISSS also shows too strong variance in some high-latitude regions, such as the Southern Ocean near the ice edge. The biases visible in the satellite results are potentially associated with the low sensitivity of orbital radiometers to SSS over cold waters, and imply that the satellite measurements must be supplemented by *in situ* observations when studying the salinity variability at mid to high latitudes. Within the tropical Atlantic, HR and LR prominently underestimate the salinity variance near the Amazon and Congo River estuaries relative to Argo and satellite estimates, potentially reflecting shortcomings with the CESM river runoff scheme. The simulations also misrepresent large-scale patterns at the Indo-Pacific Warm Pool that can be associated with documented CESM biases on the representation of the ITCZ, tropical cyclones, and intraseasonal forms of atmospheric variability such as Madden-Julian Oscillations.

Finally, we show that the larger extratropical, upper-ocean salinity variance in HR is associated with a more significant contribution of ocean advection relative to LR, predominantly attributed to the action of resolved mesoscale ocean phenomena in HR. The HR simulation also shows a better-resolved signature of atmospheric features in both its advection and surface flux-driven components, suggesting that the resolution of the atmospheric grid also influences the salinity variability. In particular, recent findings by Light et al. (2022) showed that the precipitation resolved by coupled models is jointly sensitive to the horizontal resolution of both the ocean and atmospheric grids, suggesting that realistically resolving the SSS variability in climate simulations require high resolution in both the ocean and atmosphere model components.

## Data Availability Statement

The OISSS data (Melnichenko et al., 2016, 2021; Melnichenko, 2021) is distributed by the Jet Propulsion Laboratory / Physical Oceanography Distributed Active Archive Center (JPL/PO.DAAC) at `https://doi.org/10.5067/SMP10-4U7CS`. The Argo salinity profiles (Argo, 2000; Wong et al., 2020) are quality-controlled as described in Good et al. (2013) and distributed as part of the EN.4.2.2 dataset available at `https://www.metoffice.gov.uk/hadobs/en4/`, which is ©British Crown Copyright, Met Office, 2023, provided under a Non-Commercial Government Licence (`http://www.nationalarchives.gov.uk/doc/non-commercial-government-licence/version/2/`). The Argo profiles were collected and made freely available by the International Argo Program and the national programs that contribute to it. The Argo Program is part of the Global Ocean Observing System. Lastly, the CESM outputs are described in Chang et al. (2020) and were obtained from the International Laboratory for High-Resolution Earth System Prediction (iHESP) GitHub repository at `https://ihesp.github.io/archive/products/ds_archive/Sunway_Runs.html`.

## Acknowledgments

This research was supported by NASA (80NSSC22K1283). Ben P. Kirtman, the William R. Middelthon III Endowed Chair of Earth Sciences, is grateful for the associated support and acknowledges funding from NOAA (NA20OAR4320472, NA22OAR4310603, NA23OAR4590383) and NSF (AGS2241538). All authors thank Frank Bryan and Keith Lindsey for their help in interpreting the CESM salt budget outputs.

## References


Adler, R. F., Huffman, G. J., Chang, A., Ferraro, R., Xie, P.-P., Janowiak, J., ... Nelkin, E. (2003). The version-2 Global Precipitation Climatology Project (GPCP) monthly precipitation analysis (1979–present). *Journal of Hydrometeorology*, *4*, 1147–1167. doi: https://doi.org/10.1175/1525-7541(2003)004⟨1147:TVGPCP⟩2.0.CO;2

Amores, A., Melnichenko, O., & Maximenko, N. (2017). Coherent mesoscale eddies in the North Atlantic subtropical gyre: 3-D structure and transport with application to the salinity maximum. *Journal of Geophysical Research: Oceans*, *122*(1), 23-41. doi: https://doi.org/10.1002/2016JC012256

Argo. (2000). *Argo float data and metadata from Global Data Assembly Centre (Argo GDAC).* SEANOE. doi: https://doi.org/10.17882/42182.

Bryan, F. O., & Bachman, S. (2015). Isohaline salinity budget of the North Atlantic salinity maximum. *Journal of Physical Oceanography*, *45*, 724-736. doi: https://doi.org/10.1175/JPO-D-14-0172.1

Busecke, J., Gordon, A. L., Li, Z., Bingham, F. M., & Font, J. (2014). Subtropical surface layer salinity budget and the role of mesoscale turbulence. *Journal of Geophysical Research: Oceans*, *119*(7), 4124-4140. doi: https://doi.org/10.1002/2013JC009715

Centurioni, L. R., Hormann, V., Chao, Y., Reverdin, G., Font, J., & Lee, D. (2015). Sea surface salinity observations with Lagrangian drifters in the tropical North Atlantic during SPURS: Circulation, fluxes, and comparisons with remotely sensed salinity from Aquarius. *Oceanography*, *28*(1), 96-105. doi: http://dx.doi.org/10.5670/oceanog.2015.08

Chang, P., Zhang, S., Danabasoglu, G., Yeager, S. G., Fu, H., Wang, H., ... Wu, L. (2020). An unprecedented set of high-resolution earth system simulations for understanding multiscale interactions in climate variability and change. *Journal of Advances in Modeling Earth System*, *12*(12), e2020MS002298. doi: https://doi.org/10.1029/2020MS002298

Chelton, D. B., Schlax, M. G., & Samelson, R. M. (2011). Global observations of nonlinear mesoscale eddies. *Progress in Oceanography*, *91*(2), 167-216. doi: https://doi.org/10.1016/j.pocean.2011.01.002

De Deckker, P. (2016). The Indo-Pacific Warm Pool: critical to world oceanography and world climate. *Geoscience Letters*, *3*(1), 20 pp. doi: https://doi.org/10.1186/s40562-016-0054-3

Delworth, T. L., Rosati, A., Anderson, W., Adcroft, A. J., Balaji, V., Benson, R., ... Zhang, R. (2012). Simulated climate and climate change in the gfdl cm2.5

high-resolution coupled climate model. *Journal of Climate*, *25*(8), 2755 - 2781. doi: https://doi.org/10.1175/JCLI-D-11-00316.1

Dinnat, E. P., Le Vine, D. M., Boutin, J., Meissner, T., & Lagerloef, G. (2019). Remote sensing of sea surface salinity: Comparison of satellite and in situ observations and impact of retrieval parameters. *Radio Science*, *11*(7). doi: https://doi.org/10.3390/rs11070750

Dohan, K., Kao, H., & Lagerloef, G. S. E. (2015). The freshwater balance over the North Atlantic SPURS domain from Aquarius satellite salinity, OSCAR satellite surface currents, and some simplified approaches. *Oceanography*, *28*(1), 86-95. doi: http://dx.doi.org/10.5670/oceanog.2015.07

Dong, S., Goni, G., & Lumpkin, R. (2015). Mixed-layer salinity budget in the SPURS region on seasonal to interannual time scales. *Oceanography*, *28*(1), 78-85. doi: http://dx.doi.org/10.5670/oceanog.2015.05

Farrar, J. T., & Plueddemann, A. J. (2019). On the factors driving upper-ocean salinity variability at the western edge of the Eastern Pacific Fresh Pool. *Oceanography*, *32*(2), 30-39. doi: https://doi.org/10.5670/oceanog.2019.209

Farrar, J. T., Rainville, L., Plueddemann, A. J., Kessler, W. S., Lee, C., Hodges, B. A., ... Fratantoni, D. M. (2015). Salinity and temperature balances at the SPURS central mooring during fall and winter. *Oceanography*, *28*(1), 56-65. doi: https://doi.org/10.5670/oceanog.2015.06

Fournier, S., & Lee, T. (2021). Seasonal and interannual variability of sea surface salinity near major river mouths of the world ocean inferred from gridded satellite and in-situ salinity products. *Remote Sensing*, *13*(4), 728. doi: https://doi.org/10.3390/rs13040728

Frenger, I., Gruber, N., Knutti, R., & Münnich, M. (2013). Imprint of Southern Ocean eddies on winds, clouds and rainfall. *Nature Geoscience*, *6*, 608–612. doi: https://doi.org/10.1038/NGEO1863

Gent, P. R., & McWilliams, J. C. (1990). Isopycnal mixing in ocean circulation models. *Journal of Physical Oceanography*, *20*(1), 150–155. doi: https://doi.org/10.1175/1520-0485(1990)020⟨0150:IMIOCM⟩2.0.CO;2

Good, S. A., Martin, M. J., & Rayner, N. A. (2013). EN4: Quality controlled ocean temperature and salinity profiles and monthly objective analyses with uncertainty estimates. *Journal of Geophysical Research: Oceans*, *118*(12), 6704-6716. doi: https://doi.org/10.1002/2013JC009067

Gordon, A. L., & Giulivi, C. F. (2014). Ocean eddy freshwater flux convergence into the North Atlantic subtropics. *Journal of Geophysical Research: Oceans*, *119*(6), 3327-3335. doi: https://doi.org/10.1002/2013JC009596

Kamenkovich, I. V., & Sarachik, E. S. (2004). Reducing errors in temperature and salinity in an ocean model forced by restoring boundary conditions. *Journal of Physical Oceanography*, *34*(8), 1856 - 1869. doi: https://doi.org/10.1175/1520-0485(2004)034⟨1856:REITAS⟩2.0.CO;2

Kirtman, B. P., Bitz, C., Bryan, F., Collins, W., Dennis, J., Hearn, N., … Vertenstein, M. (2012). Impact of ocean model resolution on CCSM climate simulations. *Climate Dynamics*, *39*(6), 1303-1328. doi: https://doi.org/10.1007/s00382-012-1500-3

Klein, L., & Swift, C. (1977). An improved model for the dielectric constant of sea water at microwave frequencies. *IEEE Journal of Oceanic Engineering*, *2*(1), 104-111. doi: https://doi.org/10.1109/JOE.1977.1145319

Larson, S. M., Vimont, D. J., Clement, A. C., & Kirtman, B. P. (2018). How momentum coupling affects SST variance and large-scale Pacific climate variability in CESM. *Journal of Climate*, *31*(7), 2927 - 2944. doi: https://doi.org/10.1175/JCLI-D-17-0645.1

Laurindo, L. C., Mariano, A. J., & Lumpkin, R. (2017). An improved near-surface velocity climatology for the global ocean from drifter observations. *Deep Sea Research Part I: Oceanographic Research Papers*, *124*, 73-92. doi: https://doi.org/10.1016/j.dsr.2017.04.009

Laurindo, L. C., Siqueira, L., Mariano, A. J., & Kirtman, B. P. (2019). Cross-spectral analysis of the SST/10-m wind speed coupling resolved by satellite products and climate model simulations. *Climate Dynamics*, *52*(9), 5071–5098. doi: https://doi.org/10.1007/s00382-018-4434-6

Laurindo, L. C., Small, R. J., Thompson, L., Siqueira, L., Bryan, F. O., Chang, P., … Zhang, S. (2022). Role of ocean and atmosphere variability in scale-dependent thermodynamic air-sea interactions. *Journal of Geophysical Research: Oceans*, *127*(7), e2021JC018340. doi: https://doi.org/10.1029/2021JC018340

Light, C. X., Arbic, B. K., Martin, P. E., Brodeau, L., Farrar, J. T., Griffies, S. M., … Strobach, E. (2022). Effects of grid spacing on high-frequency precipitation variance in coupled high-resolution global ocean–atmosphere models. *Climate Dynamics*, *59*(9), 2887–2913. doi: https://doi.org/10.1007/s00382-022-06257-6

Lindstrom, E., Bryan, F., & Schmitt, R. (2015). SPURS: Salinity Processes in the Upper-ocean Regional Study — The North Atlantic Experiment. *Oceanography*, *28*(1), 14-19. doi: https://doi.org/10.5670/oceanog.2015.01

Lindstrom, E., Edson, J. B., Schanze, J. J., & Shcherbina, A. Y. (2019). SPURS-

2: Salinity Processes in the Upper-ocean Regional Study — The Eastern Equatorial Pacific Experiment. *Oceanography*, *32*(2), 15-18. doi: https://doi.org/10.5670/oceanog.2019.207

Lumpkin, R., & Johnson, G. C. (2013). Global ocean surface velocities from drifters: Mean, variance, El Niño–Southern Oscillation response, and seasonal cycle. *Journal of Geophysical Research: Oceans*, *118*(6), 2992-3006. doi: https://doi.org/10.1002/jgrc.20210

Martin, P. E., Arbic, B. K., & Hogg, A. M. (2021). Drivers of atmospheric and oceanic surface temperature variance: A frequency domain approach. *Journal of Climate*, *34*(10), 3975-3990. doi: https://doi.org/10.1175/JCLI-D-20-0557.1

Meehl, G. A., Yang, D., Arblaster, J. M., Bates, S. C., Rosenbloom, N., Neale, R., … Danabasoglu, G. (2019). Effects of model resolution, physics, and coupling on southern hemisphere storm tracks in CESM1.3. *Geophysical Research Letters*, *46*(21), 12408-12416. doi: https://doi.org/10.1029/2019GL084057

Meissner, T., Wentz, F. J., & Le Vine, D. M. (2018). The salinity retrieval algorithms for the NASA Aquarius Version 5 and SMAP Version 3 releases. *Radio Science*, *10*(7). doi: https://doi.org/10.3390/rs10071121

Melnichenko, O. (2021). *Multi-mission L4 Optimally Interpoated Sea Surface Salinity. Ver. 1.0.* PO.DAAC, CA, USA. (Dataset accessed 2023-08-01 at https://doi.org/10.5067/SMP10-4U7CS)

Melnichenko, O., Amores, A., Maximenko, N., Hacker, P., & Potemra, J. (2017). Signature of mesoscale eddies in satellite sea surface salinity data. *Journal of Geophysical Research: Oceans*, *122*(2), 1416-1424. doi: https://doi.org/10.1002/2016JC012420

Melnichenko, O., Hacker, P., Bingham, F. M., & Lee, T. (2019). Patterns of SSS variability in the eastern tropical Pacific: Intraseasonal to interannual timescales from seven years of NASA satellite data. *Oceanography*, *32*(2), 20-29. doi: https://doi.org/10.5670/oceanog.2019.208

Melnichenko, O., Hacker., P., N. Maximenko, G. L., & Potemra, J. (2016). Optimal interpolation of Aquarius sea surface salinity. *Journal of Geophysical Research: Oceans*, *121*, 602-616. doi: https://doi.org/10.1002/2015JC011343

Melnichenko, O., Hacker, P., Potemra, J., Meissner, T., & Wentz, F. (2021). *Aquarius/SMAP sea surface salinity optimum interpolation analysis.* IPRC Technical Note. (No. 7, May 7, 2021)

Patrizio, C. R., & Thompson, D. W. J. (2021). Quantifying the role of ocean dynamics in ocean mixed-layer temperature variability. *Journal of Climate*(34), 2567-2589. doi: https://doi.org/10.1175/JCLI-D-20-0476.1

Patrizio, C. R., & Thompson, D. W. J. (2022). Understanding the role of ocean dynamics in midlatitude sea surface temperature variability using a simple stochastic climate model. *Journal of Climate*(35), 3313-3333. doi: https://doi.org/10.1175/JCLI-D-21-0184.1

Putrasahan, D. A., Kamenkovich, I., Le Hénaff, M., & Kirtman, B. P. (2017). Importance of ocean mesoscale variability for air-sea interactions in the Gulf of Mexico. *Geophysical Research Letters*, *44*, 6352-6362. doi: https://doi.org/10.1002/2017GL072884

Small, R. J., Bacmeister, J., Bailey, D., Baker, A., Bishop, S., Bryan, F., … Vertenstein, M. (2014). A new synoptic scale resolving global climate simulation using the Community Earth System Model. *Journal of Advances in Modeling Earth System*, *6*, 1065–1094. doi: https://doi.org/10.1002/2014MS000363

Small, R. J., Bryan, F. O., Bishop, S. P., Larson, S., & Tomas, R. A. (2020). What drives upper-ocean temperature variability in coupled climate models and observations. *Journal of Climate*, *33*, 577-596. doi: https://doi.org/10.1175/JCLI-D-19-0295.1

Small, R. J., Bryan, F. O., Bishop, S. P., & Tomas, R. A. (2019). Air–sea turbulent heat fluxes in climate models and observational analyses: What drives their variability? *Journal of Climate*, *32*(8), 2397 - 2421. doi: https://doi.org/10.1175/JCLI-D-18-0576.1

Smith, R., Jones, P., Briegleb, B., Bryan, F., Danabasoglu, G., Dennis, J., … Yeager, S. (2010). *The Parallel Ocean Program (POP) Reference Manual.* Los Alamos National Laboratory Tech. Rep. LAUR-10-01853. (141 pp.)

Spall, M. A. (1993). Variability of sea surface salinity in stochastically forced systems. *Climate Dynamics*, *8*(3), 151-160. doi: https://doi.org/10.1007/BF00208094

Stammer, D. (1998). On eddy characteristics, eddy transports, and mean flow properties. *Journal of Physical Oceanography*, *28*(4), 727 - 739. doi: https://doi.org/10.1175/1520-0485(1998)028⟨0727:OECETA⟩2.0.CO;2

Treguier, A. M., Deshayes, J., Lique, C., Dussin, R., & Molines, J. M. (2012). Eddy contributions to the meridional transport of salt in the North Atlantic. *Journal of Geophysical Research*, *117*(C5), C05010. doi: https://doi.org/10.1029/2012JC007927

Tulloch, R., Marshall, J., & Smith, K. S. (2009). Interpretation of the propagation of surface altimetric observations in terms of planetary waves and geostrophic turbulence. *Journal of Geophysical Research: Oceans*, *114*(C2).

doi: https://doi.org/10.1029/2008JC005055

Vinogradova, N., Lee, T., Boutin, J., Drushka, K., Fournier, S., Sabia, R., ... Lindstrom, E. (2019). Satellite salinity observing system: Recent discoveries and the way forward. *Frontiers in Marine Science*, *6*, 243. doi: https://doi.org/10.3389/fmars.2019.00243

Wong, A. P. S., Wijffels, S. E., Riser, S. C., Pouliquen, S., Hosoda, S., Roemmich, D., ... Park, H.-M. (2020). Argo data 1999–2019: Two million temperature-salinity profiles and subsurface velocity observations from a global array of profiling floats. *Frontiers in Marine Science*, *7*, 700. doi: https://doi.org/10.3389/fmars.2020.00700

Xie, P., Joyce, R., Wu, S., Yoo, S.-H., Yarosh, Y., Sun, F., & Lin, R. (2017). Reprocessed, bias-corrected cmorph global high-resolution precipitation estimates from 1998. *Journal of Hydrometeorology*, *18*(6). doi: https://doi.org/10.1175/JHM-D-16-0168.1

Zhang, Q., Chang, P., Yeager, S. G., Danabasoglu, G., & Zhang, S. (2022). Role of sea-surface salinity in simulating historical decadal variations of Atlantic meridional overturning circulation in a coupled climate model. *Geophysical Research Letters*, *49*(4), e2021GL096922. doi: https://doi.org/10.1029/2021GL096922

Zhang, S., Fu, H., Wu, L., Li, Y., Wang, H., Zeng, Y., ... Guo, Y. (2020). Optimizing high-resolution community earth system model on a heterogeneous many-core supercomputing platform. *Geoscientific Model Development*, *13*(10), 4809–4829. doi: https://doi.org/10.5194/gmd-13-4809-2020

**Figure 1.**

(a) OISSS
(b) Argo
(c) CESM-LR
(d) CESM-HR
90°N
60°N
30°N
0°
30°S
60°S
90°S
60°E
120°E
180°
120°W
60°W
0°
−3.5
−3.0
−2.5
−2.0
−1.5
−1.0
−0.5
0.0
Variance [log10(psu2)]

**Figure 2.**

(a)
OISSS
CESM-LR
CESM-HR
(b)
Argo
CESM-LR
CESM-HR
log10(psu2)
0.0
−0.5
−1.0
−1.5
−2.0
−2.5
−3.0
60°S
40°S
20°S
0°
20°N
40°N
60°N

**Figure 3.**

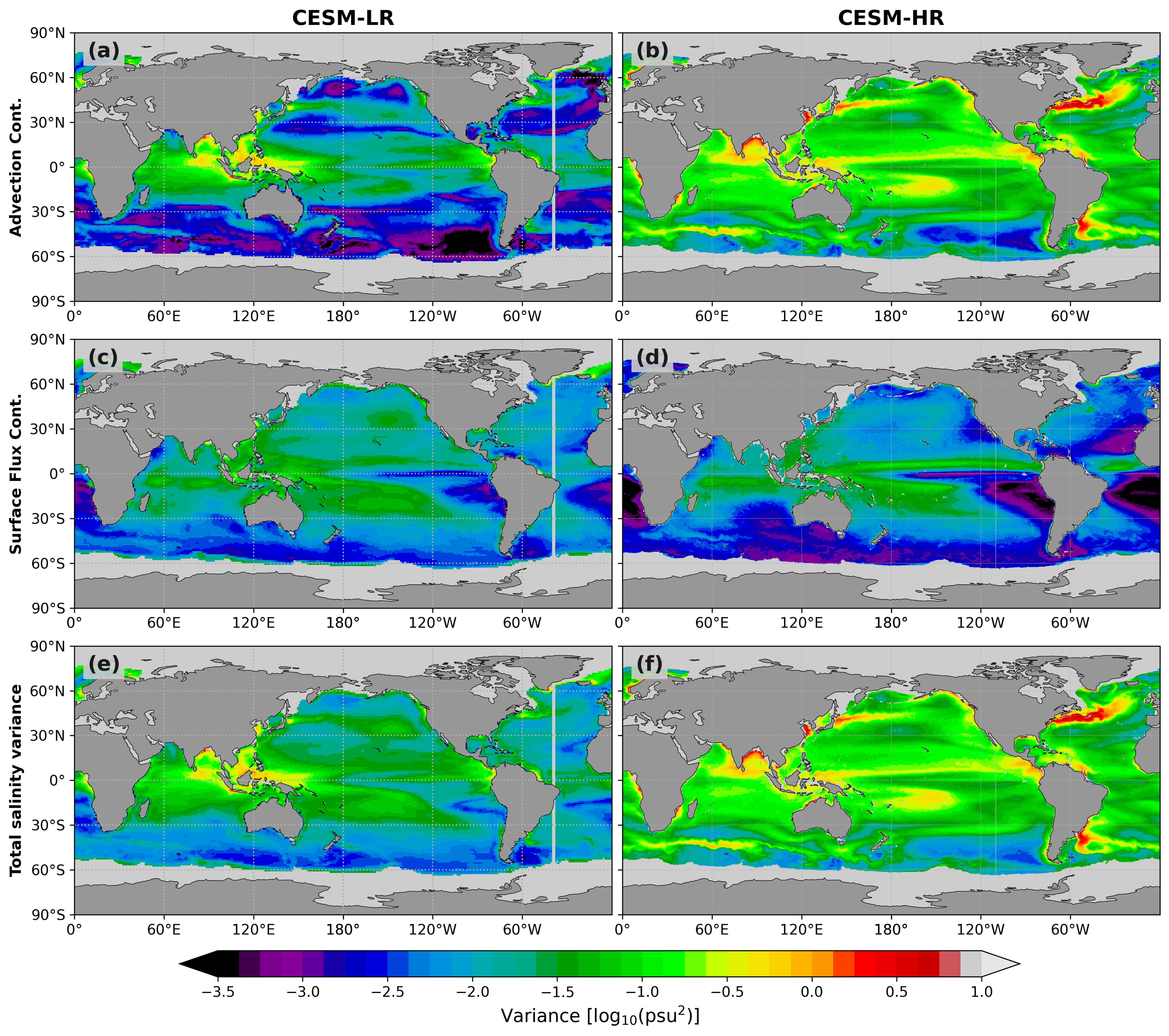

CESM-LR
CESM-HR
(a)
(b)
(c)
(d)
(e)
(f)
Advection Cont.
Surface Flux Cont.
Total salinity variance
90°N
60°N
30°N
0°
30°S
60°S
90°S
0°
60°E
120°E
180°
120°W
60°W
−3.5
−3.0
−2.5
−2.0
−1.5
−1.0
−0.5
0.0
0.5
1.0
Variance [$\log_{10}(\mathrm{psu}^2)$]

**Figure 4.**

(a) CESM-LR
(b) CESM-HR
Total variance
Advection cont.
Surface flux cont.
log10(psu2)
0.0
−0.5
−1.0
−1.5
−2.0
−2.5
−3.0
60°S
40°S
20°S
0°
20°N
40°N
60°N

# Quantifying the contribution of ocean advection and surface flux to the upper-ocean salinity variability resolved by climate model simulations

**Lucas C. Laurindo[1], Leo Siqueira[1,2], R. Justin Small[3], LuAnne Thompson[4], and Benjamin P. Kirtman[1,2,5]**

[1]Rosenstiel School of Marine, Atmospheric & Earth Science, University of Miami, Miami, FL, USA.
[2]Frost Institute for Data Science and Computing, University of Miami, Miami, FL, USA.
[3]Climate and Global Dynamics Laboratory, National Center for Atmospheric Research, Boulder, Colorado, CO, USA.
[4]School of Oceanography, University of Washington, Seattle, WA, USA.
[5]Cooperative Institute for Marine and Atmospheric Studies, University of Miami, Miami, FL, USA.

**Key Points:**

- We investigate how advection and surface flux affect upper-50-m salinity variance in eddy-resolving and eddy-parameterized climate models.
- The extratropical variance in the eddy-resolving run matches Argo and is much larger than in the eddy-parameterized run and satellite data.
- The larger upper-ocean salinity variance in the eddy-resolving run is predominantly driven by mesoscale ocean processes.

Corresponding author: Lucas C. Laurindo, `llaurindo@earth.miami.edu`

## Abstract

This study examines the impact of ocean advection and surface freshwater flux on the non-seasonal, upper-ocean salinity variability in two climate model simulations with eddy-resolving and eddy-parameterized ocean components (HR and LR, respectively). We assess the realism of each simulation by comparing their sea surface salinity (SSS) variance with satellite and Argo float estimates. Our results show that, in the extratropics, the HR variance is about five times larger than that in LR and agrees with the Argo estimates. In turn, the extratropical satellite SSS variance is smaller than that from HR and Argo by about a factor of two, potentially reflecting the low sensitivity of radiometers to SSS in cold waters. Using a simplified salinity conservation equation for the upper-50-m ocean layer, we find that the advection-driven variance in HR is, on average, one order of magnitude larger than the surface flux-driven variance, reflecting the action of mesoscale processes.



## Plain Language Summary

This study explores the importance of ocean currents, evaporation, and rainfall for driving changes in the salt concentration in the upper ocean (known as salinity) in two climate model simulations with differing ocean resolutions. The high-resolution model (HR) simulates ocean currents with dimensions of tens of km, while the low-resolution model (LR) can only simulate currents with hundreds of km in size. When comparing their simulated sea surface salinity variations with those captured by satellites and autonomous floats from the Argo array, the salinity variability in the high-resolution model is similar to the Argo data at mid to high latitudes and about five times stronger than that in the low-resolution model. The satellite data show a variability two times smaller than HR and Argo in the same regions, potentially due to low sensitivity to the surface salinity in cold waters. Using a simple equation describing the conservation of salinity in the upper ocean, we have shown that small-scale ocean currents drive most of the salinity variability in HR, while in LR, ocean currents play a much smaller role.


## 1 Introduction

Mesoscale ocean currents play a significant role in setting the upper-ocean temperature variability over much of the extratropical oceans. Indeed, estimates based on observations and model simulations indicate that the heat flux convergence associated with the mesoscale ocean eddy variability dominates over other terms of the heat budget equation at spatial scales smaller than about 1000 km and timescales ranging from intraseasonal to interannual (e.g., Putrasahan et al., 2017; Small et al., 2020; Martin et al., 2021;

Patrizio & Thompson, 2021, 2022) and potentially longer (Laurindo et al., 2022). While the conclusions drawn for the upper-ocean temperature suggest that advection by transient ocean motions can also be relevant for driving the upper-ocean salinity variability, only regional assessments of salinity have been made, and they show contrasting conclusions on the role of advection.

Results from the Salinity Processes in the Upper-ocean Regional Study (SPURS) field experiment conducted in the subtropical North Atlantic (SPURS-1, Lindstrom et al., 2015) indicate that the local time-averaged SSS is primarily balanced by the net surface fluxes acting to increase the salinity against the freshening effect of Ekman advection, seasonal fluctuations are mainly controlled by the seasonally-varying surface forcing, and interannual variations by surface fluxes and advection by Ekman currents, with little influence from mesoscale ocean processes (Dohan et al., 2015; Dong et al., 2015). In contrast, other studies show that freshwater advection by mesoscale ocean eddies contributes to the monthly to intraseasonal SSS variability in the region (Busecke et al., 2014; Centurioni et al., 2015; Farrar et al., 2015; Melnichenko et al., 2017), with model-based assessments also suggesting an important role in the time-averaged balance and on seasonal to interannual variations (Busecke et al., 2014; Gordon & Giulivi, 2014).

Treguier et al. (2012) showed that mesoscale eddies are essential for balancing the meridional freshwater transport in an eddy-resolving, 1/12° horizontal resolution ocean simulation of the North Atlantic, a mechanism that was absent in a corresponding eddy-permitting, 1/4° resolution run. The eddy-induced freshwater transport inferred by Treguier et al. (2012) was consistent with satellite and hydrography-based estimates for the region (Stammer, 1998; Amores et al., 2017; Melnichenko et al., 2017). Model results also indicate that eddy stirring enhances horizontal salinity gradients where small-scale mixing can occur (Bryan & Bachman, 2015).

In the eastern equatorial North Pacific, results from a second SPURS experiment (SPURS-2, Lindstrom et al., 2019) indicate that the local upper-ocean salinity budget is predominantly balanced by the freshening effect of the surface fluxes and the salting induced by vertical advection, with monthly to seasonal variations in the region driven by fluctuations in the Ekman advection (Farrar & Plueddemann, 2019; Melnichenko et al., 2019). In addition, satellite data indicates that westward propagating eddies contribute to the intraseasonal SSS variability in the area and that interannual changes reflect variations in the surface freshwater fluxes associated with the El Niño-Southern Oscillation (ENSO) cycle (Melnichenko et al., 2019).

The differing conclusions on the importance of mesoscale ocean currents for driving the SSS variability may stem from uncertainties of the observational datasets used, the geographical locations and size of the control volumes used, and the different temporal averaging periods used in the assessments (Lindstrom et al., 2015). The configuration of model experiments may have contributed to the divergence in the literature, as the horizontal ocean resolution controls the mesoscale current variability and the associated tracer transport (Kirtman et al., 2012; Treguier et al., 2012; Small et al., 2014; Chang et al., 2020). Further, most previous modeling studies used ocean-only simulations that cannot account for coupled ocean-atmosphere feedbacks on surface freshwater flux (e.g., Frenger et al., 2013; Light et al., 2022), and that rely on physically unrealistic sea surface salinity restoring schemes (Spall, 1993; Kamenkovich & Sarachik, 2004; Q. Zhang et al., 2022).

Here, we examine the influence of mesoscale processes on the monthly upper-ocean salinity variance at global scales from two fully coupled climate model simulations configured with eddy-resolving and eddy-parameterized ocean components. We quantify the contribution of ocean advection and surface freshwater fluxes to the upper-ocean salinity variability resolved by each simulation using saved terms in the salinity budget and assess their realism by comparing their global sea surface salinity (SSS) variance maps with that estimated using satellite and Argo float data.

Our work is organized as follows. Section 2 describes the observational products and climate model simulations (2.1), the methods applied for computing the upper-ocean salinity variance from the datasets used (2.2), and the budget equation used to decompose the model salinity variance into advection-driven and surface flux driven components (2.3). The results are presented and discussed in Section 3, while Section 4 summarizes this study and its conclusions.

# 2 Methods

## 2.1 Data description

### *2.1.1 Satellite sea surface salinity data*

We use near-global satellite SSS data for September 2011 to March 2022 from the Multi-Mission Optimally Interpolated Sea Surface Salinity dataset (OISSS, Melnichenko et al., 2016, 2021). This product combines observations from three satellites: Aquarius/SAC-D (August 2011 to June 2015), Soil Moisture Active Passive (SMAP, March 2015 until the present), and Soil Moisture and Ocean Salinity (SMOS, January 2010 to present). Their primary instruments are passive microwave radiometers that measure the surface radiative flux along wide ground swaths. The measurements are taken in the L-band radiometric frequency band ($\sim$1.4 GHz), where the equivalent surface brightness temperature is highly correlated with SSS for sea surface temperatures above 5°C (Klein & Swift, 1977). However, these correlations rapidly drop for temperatures less than 5°C (Meissner et al., 2018; Dinnat et al., 2019; Vinogradova et al., 2019). The OISSS data is produced at a $0.25° \times 0.25° \times$ 4-day grid, has a 0.19 psu root mean square difference relative to *in situ* measurements, and near-zero bias.

#### 2.1.2 Vertical salinity profiles from Argo floats

We utilize about two and a half million quality-controlled vertical salinity profiles obtained from January 1998 to December 2020 by Argo profiling floats (Good et al., 2013; Wong et al., 2020). The Argo floats are designed to drift in neutral equilibrium at 1000 or 2000 m depth, emerging every ten days to measure pressure, temperature, and salinity as they rise. After transmitting their position and data to land-based receiving stations, the floats return to their drifting depth until the next sampling cycle. The Argo array is globally distributed and currently has more than 3800 floats that gather about 12,000 profiles each month.

#### 2.1.3 CESM climate model outputs

We analyze two climate simulations produced using the Community Earth System Model version 1.3 (CESM, Meehl et al., 2019; S. Zhang et al., 2020) with differing horizontal resolutions in the ocean and atmosphere. The first is low-resolution (LR), using a nominal 1° resolution in both components that requires parameterizing the effects of mesoscale ocean processes (e.g., Gent & McWilliams, 1990). The second is high-resolution (HR), using a 0.25° resolution in the atmosphere and 0.1° in the ocean that is eddy-resolving except at high latitudes. LR is integrated for 501 years and HR for 519 years, both using 1850 $CO_2$ forcing. These simulations are thoroughly described in Chang et al. (2020).

The CESM outputs used in this work are monthly-averaged horizontal fields of SSS and surface freshwater flux, and three-dimensional monthly global fields of ocean salt flux convergence computed using horizontal and vertical advection components. The LR (HR) quantities are obtained for the simulation years 1–249 (338–519), following their availability in the model output files.

### 2.2 Estimating the salinity variance using observations and CESM data

To compute variance maps, we define salinity anomalies as fluctuations about a best-fit model composed of the long-term mean, a linear temporal trend, and of annual and semiannual harmonics representing the seasonal cycle. We first compute monthly averages of the 4-day resolution satellite SSS data for consistency with the model outputs before isolating the monthly anomalies. In turn, using model data, we estimate the SSS variance for 10-year segments of the monthly outputs to simulate the length of the satellite record. This results in twenty-one global SSS variance maps for LR and eighteen for HR, which we use to estimate the uncertainty of the SSS variance levels resolved by the simulations.

In the case of the Argo vertical salinity profiles, SSS data is unavailable as the shallowest measurements are taken at 5-m depth or more. Thus, we consider the average salinity measured by the floats over the first 10 m of the water column as a proxy for SSS, consistent with the 10-m thickness of the CESM surface ocean layer. We also low-pass filter the 10-day resolution data along the float trajectories at thirty days to reproduce the monthly sampling frequency of the model data. Finally, we use the data binning procedure described in Laurindo et al. (2017) to decompose the Argo measurements into time-mean, seasonal, and eddy components, the latter of which are used to compute a regular-gridded ($0.25^\circ \times 0.25^\circ$ resolution) global salinity variance map.

### 2.3 Decomposing the CESM upper-ocean salinity variance

Inspired by the analysis of Patrizio and Thompson (2021), here we use a simplified salinity conservation equation to diagnose the contribution of the ocean advection and surface freshwater fluxes to the monthly salinity variability in a surface layer of thickness $h = 50$-m resolved by the HR and LR simulations, given by:

$$\frac{\partial \langle S \rangle}{\partial t} = \underbrace{-\langle \nabla \cdot (\mathbf{u}S) \rangle}_{\text{Ocean advection } (Q_o)} + \underbrace{\frac{S_0}{h}(E - P)}_{\text{Surface fluxes } (Q_s)} , \tag{1}$$

where the brackets denote quantities vertically averaged over the upper 50-m, $\mathbf{u}$ is the three-dimensional velocity vector, $S$ represents salinity, $E$ evaporation, $P$ precipitation, and $S_0$ is a constant reference salinity equal to 34.7 psu. The first term on the right-hand side represents the salt flux convergence associated with the three-dimensional ocean advection ($Q_o$), and the second term the surface freshwater flux ($Q_s$). Eq. (1) omits the contributions of entrainment at the bottom of the layer and of diffusive processes.

Dropping the brackets for simplicity and isolating monthly mean anomalies (represented by primes) from (1) yields:

$$\frac{\partial S'}{\partial t} = Q'_o + Q'_s, \tag{2}$$

from which we obtain an analytical expression for the salinity variance $\sigma_S^2$ by centered differencing the salinity tendency term, squaring both sides of the equation, and taking a time average:

$$\sigma_S^2 = \frac{2\Delta t^2}{1 - r_2}\left(\overline{Q_o'^2} + \overline{Q_s'^2} + 2\overline{Q'_o Q'_s}\right), \tag{3}$$

where $\Delta t$ represents the sampling interval of one month, and $r_2$ is the two-month lag autocorrelation of the vertically-averaged salinity (Patrizio & Thompson, 2021).

From (3), we define the diagnostic relationship:

$$\sigma_S^2 = \tilde{Q}_{oo} + \tilde{Q}_{ss} + \tilde{Q}_{os}, \tag{4}$$

where $\tilde{Q}_{oo}$ and $\tilde{Q}_{ss}$ represent the contribution of ocean advection and surface freshwater flux for driving the upper-ocean salinity variability, respectively, while $\tilde{Q}_{os}$ arises from the covariance between advection and surface fluxes. They are expressed as:

$$\tilde{Q}_{oo} = \frac{2\Delta t^2}{1 - r_2}\overline{Q_o'^2}, \tag{5}$$

$$\tilde{Q}_{ss} = \frac{2\Delta t^2}{1 - r_2}\overline{Q_s'^2}, \tag{6}$$

$$\tilde{Q}_{os} = \frac{4\Delta t^2}{1 - r_2}\overline{Q'_o Q'_s}. \tag{7}$$

We use (4) to (7), combined with the salt flux convergence and surface freshwater flux outputs, to estimate $\sigma_S^2$, $\tilde{Q}_{oo}$, $\tilde{Q}_{ss}$, and $\tilde{Q}_{os}$ for HR and LR. We note that the CESM budget outputs are for the conservation of salt content rather than of salinity. While both are equivalent at subsurface layers, undulations of the free surface can strongly modulate the salt content of the surface layer but not its salinity (c.f. Sec. 3.3 of Smith et al., 2010). Since we focus on the salinity variability, here we examine advection outputs vertically-averaged over the 10 to 50 m layer as a proxy for the upper-50-m salinity flux convergence $Q_o$. We isolate the monthly anomalies $Q'_o$ and $Q'_s$ using the methods described in Sec. 2.2, which are then applied in Eqs. (4) to (7) for computing the quantities of interest.

# 3 Results and discussion

## 3.1 Salinity variance in observations and CESM simulations

Here, we compare the non-seasonal, monthly SSS variance calculated using OISSS data, Argo data, and outputs from LR and HR. The large-scale patterns observed in the OISSS data (Fig. 1a) resemble those of the long-term mean precipitation (e.g., Adler et al., 2003; Xie et al., 2017), with enhanced values found in the vicinity of the Intertropical Convergence Zone (ITCZ) in the Atlantic and Pacific basins and over much of the Indian Ocean. This may indicate the influence of transient precipitation events from small-scale convective systems. The enhanced SSS variance within the tropics can also be attributed to advection by Ekman currents and Tropical Instability Waves (Melnichenko et al., 2019). In addition, significant SSS variances are associated with the freshwater discharge of major rivers, such as the Amazon (Congo) in the western (eastern) tropical Atlantic, the La Plata in the western South Atlantic, the Mississippi in the Gulf of Mexico, and the Ganges in the Bay of Bengal (Fournier & Lee, 2021). Moving to the extratropics, enhanced SSS variance appears in strong current systems, most prominently the Gulf Stream seaward extension, and to a lesser degree in the Kuroshio Current, Brazil Current, the Brazil-Malvinas Confluence, and the Agulhas Current System. The large SSS variance in these regions coincides with strong time-mean horizontal SSS gradients, suggesting that it arises from horizontal advection by mesoscale ocean currents (Amores et al., 2017; Melnichenko et al., 2017, 2019).

The upper-10-m salinity variance from Argo (Fig. 1b) show similar spatial distribution and magnitudes within the tropics. However, the Argo estimates resolve spatial patterns associated with all major extratropical current systems that are better defined and with larger magnitudes. In particular, the Argo estimates show values of up to 1.8 psu$^2$ (whose logarithm is $\sim 0.2$, for visualization in Fig. 1) at the Gulf Stream seaward extension, compared to only 0.3 psu$^2$ in OISSS (log $\sim -0.7$). About one order of magnitude differences are also seen at the Brazil-Malvinas Confluence and the Kuroshio and Agulhas Currents. The Argo estimates further show enhanced variances associated with the Antarctic Circumpolar Current (ACC) that are absent in OISSS. Also absent are zonally-elongated variance bands of about 0.03 psu$^2$ (log $-1.5$) south of Australia and in the Pacific and Atlantic subtropical gyres. Finally, Argo prominently show wide low variance regions ($\leq$0.01 psu$^2$, or $\leq -2$ in log scale) in the Southern Ocean that coincides with low eddy kinetic energy regions (Lumpkin & Johnson, 2013).

The comparison between the LR and HR variances provides further insight into the importance of mesoscale processes. Similarly to observations (Figs. 1a-b), HR re-

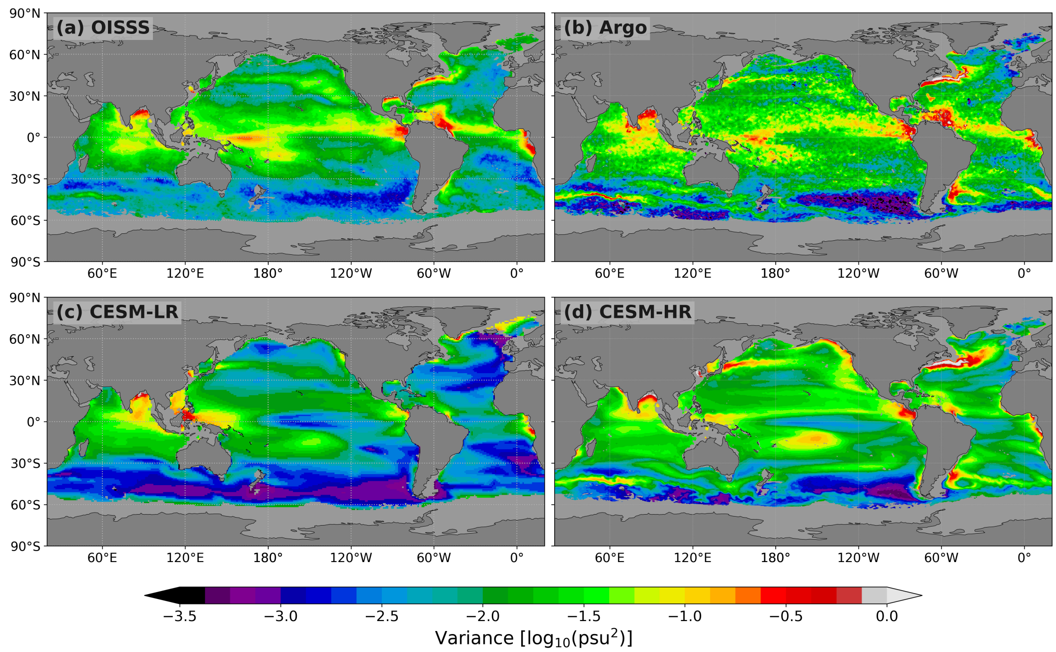


**Figure 1.** Monthly sea surface salinity (SSS) variance resolved by the OISSS satellite product (a), of the upper-10-m averaged salinity estimated using from Argo float data (b), and of the monthly SSS variance resolved by the low- and high-resolution CESM simulations (c and d). All estimates are shown in logarithmic scale.

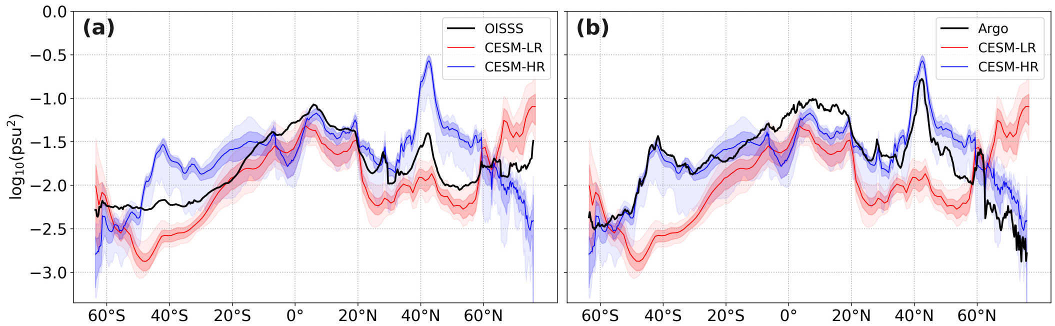


**Figure 2.** Zonally-averaged SSS variance from low- and high-resolution CESM simulations (red and blue lines, respectively), contrasted against zonally-averaged observational estimates (black lines) of the SSS variance resolved by the OISSS satellite product (panel a) and the upper-10-m salinity variance computed using Argo data (b). The darker shading around the CESM estimates is the standard deviation of the zonally-averaged salinity variances of individual ten-year segments of the model outputs, while the lighter shading show the minimum and maximum values obtained over all segments. All estimates are shown in logarithmic scale.

solves the enhanced variability associated with extratropical current systems, features absent in the LR results (Figs. 1c-d). Notably, the spatial features and variance levels resolved by HR in the extratropics resemble those shown by the Argo results.

Zonally-averaged salinity variances (Fig. 2) reinforce the similarity between the HR and Argo results in the extratropics and that both are significantly larger than those from LR. The zonally-averaged variance estimates from Argo (Fig. 2b) fall within one standard deviation of the ensemble-averaged HR variance estimates (computed as described in Sec. 2.2) in the Southern Hemisphere, and are generally larger than the minimum variance for HR in the Northern. In turn, the variance from OISSS (Fig. 2a), albeit larger than those from LR at most latitudes, are muted relative to Argo and HR between about 60°S and 55°N and exceed the variance levels resolved by both Argo and HR poleward of these latitudes. These characteristics likely reflect the smaller sensitivity of the SSS satellite retrievals in cold waters (Klein & Swift, 1977; Meissner et al., 2018; Dinnat et al., 2019; Vinogradova et al., 2019). Further highlighting the similarity between HR and Argo and their larger variance levels relative to LR and OISSS, the global area-averaged SSS variances are 0.009, 0.018, 0.021, 0.014 psu$^2$ for LR, HR, Argo, and OISSS respectively. Considering only latitudes poleward of 23°, these values change to 0.002, 0.010, 0.011, and 0.004 psu$^2$ for LR, HR, Argo, and OISSS, respectively.

Despite the higher overall realism of HR relative to LR, there are important differences relative to observations. In particular, OISSS and Argo both show larger and spatially more widespread salinity variance off the mouth of large rivers than HR, most prominently for the Amazon and Congo, potentially reflecting issues with the river runoff scheme in CESM-HR. Observations also show local salinity variance maxima in the western tropical Pacific, associated with the Indo-Pacific Warm Pool (De Deckker, 2016), that are imperfectly reproduced in HR. Specifically, the HR shows high variance values over the equator that are shifted west and closer to Indonesia relative to that from OISSS and Argo, while the high variances centered at about 10°S are shifted east by almost thirty degrees. These biases can be associated with deficiencies in how CESM represents atmospheric phenomena within the tropics, such as Madden-Julian Oscillations, tropical cyclones, and the ITCZ, as documented in Chang et al. (2020).

### 3.2 Role of advection and surface flux in the CESM salinity variance

In this Section, we examine the contribution of ocean advection and surface freshwater fluxes to the upper-50-m salinity variance, as resolved by HR and LR simulations, using Eqs. (4) to (7). The advection-induced salinity variance [$\tilde{Q}_{oo}$, Eq. (5)] is much higher in HR than in LR, except in the Indo-Pacific Warm Pool and in the eastern tropical Pacific, where both simulations show comparable values (Figs. 3a-b). The contribution of surface freshwater fluxes [$\tilde{Q}_{ss}$, Eq. (6)] is similar in both simulations, except in the Southern Ocean and in the western portion of the oceanic basins, where it can be up to one order of magnitude larger in LR relative to HR (Figs. 3c-d). The spatial distribution of the surface flux-induced variance is similar to climatological precipitation (e.g., Adler et al., 2003; Xie et al., 2017). The contribution of the covariance between advection and surface fluxes to the total salinity variance [$\tilde{Q}_{os}$, Eq. (7)] is smaller in magnitude than the other two components and shows predominantly negative values, whose spatial distribution mirrors that of the surface fluxes (Fig. S1). The global area-averaged values of the advection, surface flux, and covariance components are 0.019, 0.010, and −0.003 psu$^2$ for LR, in contrast to 0.092, 0.007, and −0.005 psu$^2$ for HR.

The sum of all components [$\sigma_S^2$, Eq. (4), Figs. 3e-f] produce salinity variance fields for LR and HR with spatial features similar to the respective monthly SSS variance fields (Figs. 3c-d), although with larger magnitudes, especially for HR. This is because $\sigma_S^2$ is obtained from monthly-averaged outputs of advection and surface freshwater flux, which are components of the salinity tendency that result from the difference between the instantaneous salinity from the beginning and end of each simulation month, while the SSS variances are computed using monthly-averaged salinity outputs that attenuate high-frequency

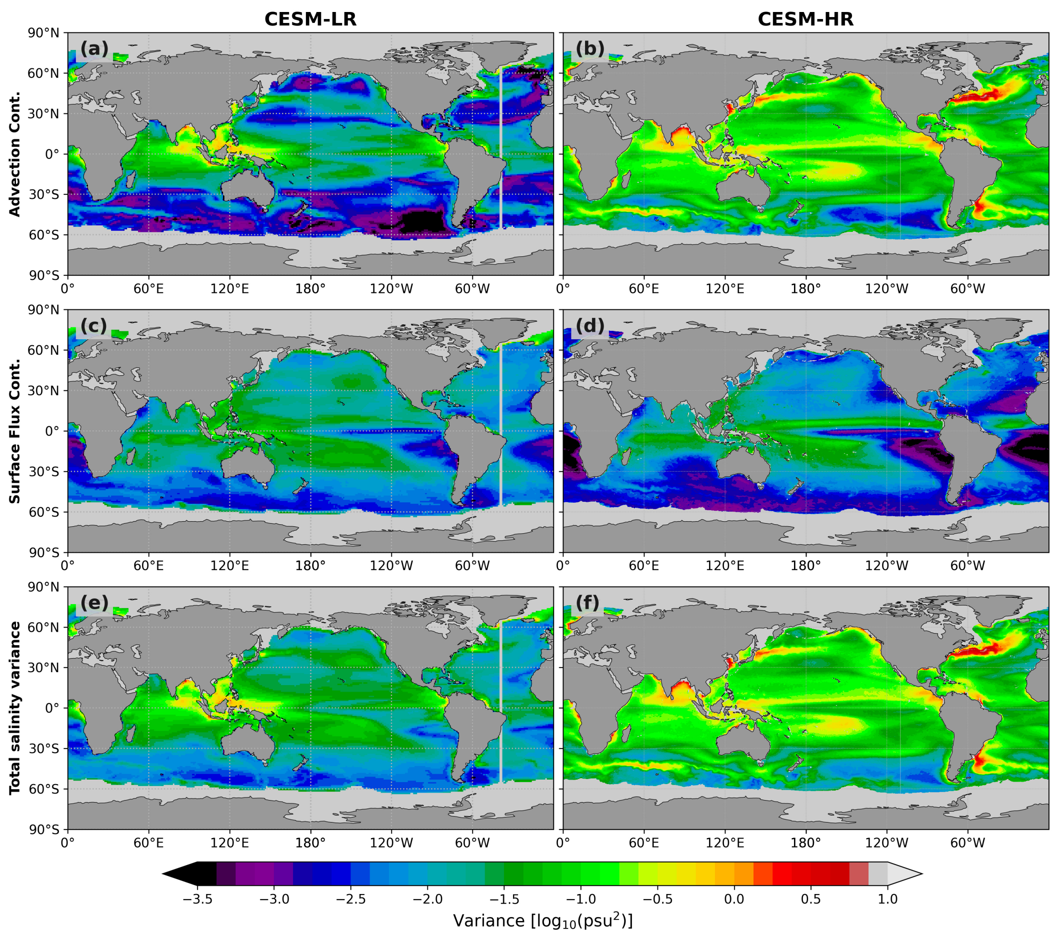


**Figure 3.** Contribution of ocean advection (a, b) and of surface freshwater fluxes (c, d) to the upper-50 m salinity variance (e, f) resolved by the low- and high-resolution CESM simulations. All estimates are shown in logarithmic scale.

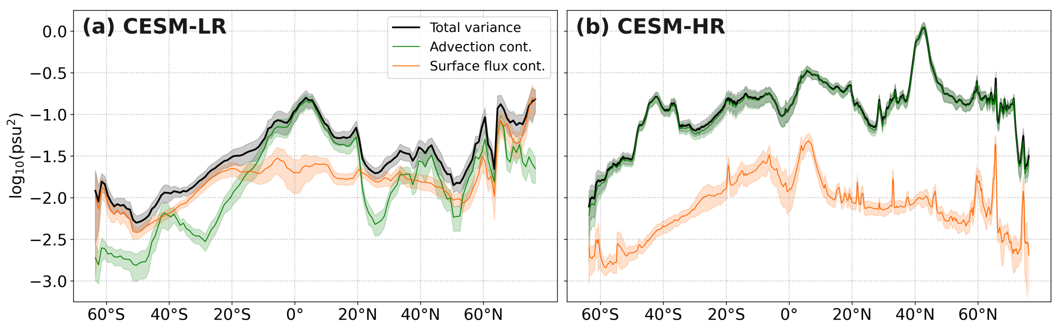


**Figure 4.** Zonally-averaged contributions of ocean advection and surface freshwater flux (orange and green lines, respectively) to the total salinity variance (black lines) for the low- and high-resolution CESM simulations (panels a and b, respectively). The shading around the estimates are the standard deviation of the zonally-averaged variances computed for individual ten-year segments of the model outputs. Estimates are shown in logarithmic scale.

variability. Here, the global area-average variances and 0.026 psu$^2$ for LR and 0.094 psu$^2$ for HR, about three and five times larger, respectively, than the corresponding values obtained for SSS.

Specifically in LR, the upper-ocean salinity variance is dominated by advection within the tropics and at western boundary currents, and by surface fluxes in the Southern Ocean and at the interior of all subtropical gyres (Fig. 3). Zonal averages of the advection- and surface-flux-induced salinity variance further highlights that surface fluxes predominantly drive the variance south of 20°S while north of 20°N both components contribute about equally (Fig. 4). In turn, the HR salinity variance is dominated by advection virtually everywhere, with a contribution from the surface fluxes only noticeable at quiescent, low salinity variance regions in the Southern Ocean (Figs. 3 and 4).

These results show that the larger upper-ocean salinity variance levels in HR are due to larger advective flux variability compared to LR. The advective fluxes consist of Ekman and geostrophic components, with the Ekman dynamics being forced by the atmosphere via wind stress and contributing to the SST variability within the tropics (Larson et al., 2018; Small et al., 2020). Geostrophic current variability near the equator is explained by large-scale, equatorially-trapped waves such as Rossby and Tropical Instability Waves, while in the extratropics it is explained by mesoscale eddies (Tulloch et al., 2009; Chelton et al., 2011), which dominate the non-seasonal SST variability in eddy-resolving simulations (Delworth et al., 2012; Kirtman et al., 2012; Putrasahan et al., 2017; Small et al., 2020; Laurindo et al., 2022).

We note that the simulations also have different horizontal atmospheric resolutions (0.25° vs. 1°), which enables a more accurate representation of phenomena such as weather fronts and tropical cyclones in HR. These phenomena significantly affect precipitation (Chang et al., 2020; Light et al., 2022) and likely also impact the upper-ocean salinity variance. The outline of the ITCZ in the tropical Pacific, seen in all variance components calculated using HR data [Eq. (4) and Figs. 3 and S1], is a potential signature of the influence of resolved atmospheric phenomena. This feature is weaker in LR. Previous studies have demonstrated that the influence of intrinsic ocean and atmosphere phenomena on upper-ocean temperature can be distinguished by the spatial and temporal scales where they operate (Small et al., 2019, 2020; Laurindo et al., 2019, 2022). Future studies can potentially apply similar methods to disentangle the influence of atmospheric and oceanic processes in the upper-ocean salinity variability.

## 4 Summary and conclusions

In this study, we use a simplified salinity conservation equation to quantify the contribution of ocean advection and surface freshwater flux to the non-seasonal, upper-50-m ocean salinity variability resolved by century-long CESM simulations configured with eddy-resolving and eddy-parameterized ocean resolutions (HR and LR, respectively). We determine the overall realism of each model run by contrasting their SSS variance with those calculated using ten years of satellite SSS data from the OISSS product and twenty-one years of upper-10-m averaged salinity data from Argo floats.

We find that the upper-ocean salinity variance in HR is, on average, twice as large as that from LR. The difference increases to a factor of five if we only consider the extratropics. The most significant differences occur in western boundary current systems and the ACC, where the variance can be one order of magnitude larger in HR. Relative to observations, the variance level resolved by HR is in excellent agreement in the extratropics with that estimated using Argo data and is two times larger than the OISSS satellite estimates. OISSS also shows too strong variance in some high-latitude regions, such as the Southern Ocean near the ice edge. The biases visible in the satellite results are potentially associated with the low sensitivity of orbital radiometers to SSS over cold waters, and imply that the satellite measurements must be supplemented by *in situ* observations when studying the salinity variability at mid to high latitudes. Within the tropical Atlantic, HR and LR prominently underestimate the salinity variance near the Amazon and Congo River estuaries relative to Argo and satellite estimates, potentially reflecting shortcomings with the CESM river runoff scheme. The simulations also misrepresent large-scale patterns at the Indo-Pacific Warm Pool that can be associated with documented CESM biases on the representation of the ITCZ, tropical cyclones, and intraseasonal forms of atmospheric variability such as Madden-Julian Oscillations.

Finally, we show that the larger extratropical, upper-ocean salinity variance in HR is associated with a more significant contribution of ocean advection relative to LR, predominantly attributed to the action of resolved mesoscale ocean phenomena in HR. The HR simulation also shows a better-resolved signature of atmospheric features in both its advection and surface flux-driven components, suggesting that the resolution of the atmospheric grid also influences the salinity variability. In particular, recent findings by Light et al. (2022) showed that the precipitation resolved by coupled models is jointly sensitive to the horizontal resolution of both the ocean and atmospheric grids, suggesting that realistically resolving the SSS variability in climate simulations require high resolution in both the ocean and atmosphere model components.

## Data Availability Statement

The OISSS data (Melnichenko et al., 2016, 2021; Melnichenko, 2021) is distributed by the Jet Propulsion Laboratory / Physical Oceanography Distributed Active Archive Center (JPL/PO.DAAC) at `https://doi.org/10.5067/SMP10-4U7CS`. The Argo salinity profiles (Argo, 2000; Wong et al., 2020) are quality-controlled as described in Good et al. (2013) and distributed as part of the EN.4.2.2 dataset available at `https://www.metoffice.gov.uk/hadobs/en4/`, which is ©British Crown Copyright, Met Office, 2023, provided under a Non-Commercial Government Licence (`http://www.nationalarchives.gov.uk/doc/non-commercial-government-licence/version/2/`). The Argo profiles were collected and made freely available by the International Argo Program and the national programs that contribute to it. The Argo Program is part of the Global Ocean Observing System. Lastly, the CESM outputs are described in Chang et al. (2020) and were obtained from the International Laboratory for High-Resolution Earth System Prediction (iHESP) GitHub repository at `https://ihesp.github.io/archive/products/ds_archive/Sunway_Runs.html`.

## Acknowledgments

This research was supported by NASA (80NSSC22K1283). Ben P. Kirtman, the William R. Middelthon III Endowed Chair of Earth Sciences, is grateful for the associated support and acknowledges funding from NOAA (NA20OAR4320472, NA22OAR4310603, NA23OAR4590383) and NSF (AGS2241538). All authors thank Frank Bryan and Keith Lindsey for their help in interpreting the CESM salt budget outputs.

## References


Adler, R. F., Huffman, G. J., Chang, A., Ferraro, R., Xie, P.-P., Janowiak, J., . . . Nelkin, E. (2003). The version-2 Global Precipitation Climatology Project (GPCP) monthly precipitation analysis (1979–present). *Journal of Hydrometeorology*, *4*, 1147–1167. doi: https://doi.org/10.1175/1525-7541(2003)004⟨1147:TVGPCP⟩2.0.CO;2

Amores, A., Melnichenko, O., & Maximenko, N. (2017). Coherent mesoscale eddies in the North Atlantic subtropical gyre: 3-D structure and transport with application to the salinity maximum. *Journal of Geophysical Research: Oceans*, *122*(1), 23-41. doi: https://doi.org/10.1002/2016JC012256

Argo. (2000). *Argo float data and metadata from Global Data Assembly Centre (Argo GDAC).* SEANOE. doi: https://doi.org/10.17882/42182.

Bryan, F. O., & Bachman, S. (2015). Isohaline salinity budget of the North Atlantic salinity maximum. *Journal of Physical Oceanography*, *45*, 724-736. doi: https://doi.org/10.1175/JPO-D-14-0172.1

Busecke, J., Gordon, A. L., Li, Z., Bingham, F. M., & Font, J. (2014). Subtropical surface layer salinity budget and the role of mesoscale turbulence. *Journal of Geophysical Research: Oceans*, *119*(7), 4124-4140. doi: https://doi.org/10.1002/2013JC009715

Centurioni, L. R., Hormann, V., Chao, Y., Reverdin, G., Font, J., & Lee, D. (2015). Sea surface salinity observations with Lagrangian drifters in the tropical North Atlantic during SPURS: Circulation, fluxes, and comparisons with remotely sensed salinity from Aquarius. *Oceanography*, *28*(1), 96-105. doi: http://dx.doi.org/10.5670/oceanog.2015.08

Chang, P., Zhang, S., Danabasoglu, G., Yeager, S. G., Fu, H., Wang, H., . . . Wu, L. (2020). An unprecedented set of high-resolution earth system simulations for understanding multiscale interactions in climate variability and change. *Journal of Advances in Modeling Earth System*, *12*(12), e2020MS002298. doi: https://doi.org/10.1029/2020MS002298

Chelton, D. B., Schlax, M. G., & Samelson, R. M. (2011). Global observations of nonlinear mesoscale eddies. *Progress in Oceanography*, *91*(2), 167-216. doi: https://doi.org/10.1016/j.pocean.2011.01.002

De Deckker, P. (2016). The Indo-Pacific Warm Pool: critical to world oceanography and world climate. *Geoscience Letters*, *3*(1), 20 pp. doi: https://doi.org/10.1186/s40562-016-0054-3

Delworth, T. L., Rosati, A., Anderson, W., Adcroft, A. J., Balaji, V., Benson, R., . . . Zhang, R. (2012). Simulated climate and climate change in the gfdl cm2.5

high-resolution coupled climate model. *Journal of Climate*, *25*(8), 2755 - 2781. doi: https://doi.org/10.1175/JCLI-D-11-00316.1

Dinnat, E. P., Le Vine, D. M., Boutin, J., Meissner, T., & Lagerloef, G. (2019). Remote sensing of sea surface salinity: Comparison of satellite and in situ observations and impact of retrieval parameters. *Radio Science*, *11*(7). doi: https://doi.org/10.3390/rs11070750

Dohan, K., Kao, H., & Lagerloef, G. S. E. (2015). The freshwater balance over the North Atlantic SPURS domain from Aquarius satellite salinity, OSCAR satellite surface currents, and some simplified approaches. *Oceanography*, *28*(1), 86-95. doi: http://dx.doi.org/10.5670/oceanog.2015.07

Dong, S., Goni, G., & Lumpkin, R. (2015). Mixed-layer salinity budget in the SPURS region on seasonal to interannual time scales. *Oceanography*, *28*(1), 78-85. doi: http://dx.doi.org/10.5670/oceanog.2015.05

Farrar, J. T., & Plueddemann, A. J. (2019). On the factors driving upper-ocean salinity variability at the western edge of the Eastern Pacific Fresh Pool. *Oceanography*, *32*(2), 30-39. doi: https://doi.org/10.5670/oceanog.2019.209

Farrar, J. T., Rainville, L., Plueddemann, A. J., Kessler, W. S., Lee, C., Hodges, B. A., … Fratantoni, D. M. (2015). Salinity and temperature balances at the SPURS central mooring during fall and winter. *Oceanography*, *28*(1), 56-65. doi: https://doi.org/10.5670/oceanog.2015.06

Fournier, S., & Lee, T. (2021). Seasonal and interannual variability of sea surface salinity near major river mouths of the world ocean inferred from gridded satellite and in-situ salinity products. *Remote Sensing*, *13*(4), 728. doi: https://doi.org/10.3390/rs13040728

Frenger, I., Gruber, N., Knutti, R., & Münnich, M. (2013). Imprint of Southern Ocean eddies on winds, clouds and rainfall. *Nature Geoscience*, *6*, 608–612. doi: https://doi.org/10.1038/NGEO1863

Gent, P. R., & McWilliams, J. C. (1990). Isopycnal mixing in ocean circulation models. *Journal of Physical Oceanography*, *20*(1), 150–155. doi: https://doi.org/10.1175/1520-0485(1990)020⟨0150:IMIOCM⟩2.0.CO;2

Good, S. A., Martin, M. J., & Rayner, N. A. (2013). EN4: Quality controlled ocean temperature and salinity profiles and monthly objective analyses with uncertainty estimates. *Journal of Geophysical Research: Oceans*, *118*(12), 6704-6716. doi: https://doi.org/10.1002/2013JC009067

Gordon, A. L., & Giulivi, C. F. (2014). Ocean eddy freshwater flux convergence into the North Atlantic subtropics. *Journal of Geophysical Research: Oceans*, *119*(6), 3327-3335. doi: https://doi.org/10.1002/2013JC009596

Kamenkovich, I. V., & Sarachik, E. S. (2004). Reducing errors in temperature and salinity in an ocean model forced by restoring boundary conditions. *Journal of Physical Oceanography*, *34*(8), 1856 - 1869. doi: https://doi.org/10.1175/1520-0485(2004)034⟨1856:REITAS⟩2.0.CO;2

Kirtman, B. P., Bitz, C., Bryan, F., Collins, W., Dennis, J., Hearn, N., ... Vertenstein, M. (2012). Impact of ocean model resolution on CCSM climate simulations. *Climate Dynamics*, *39*(6), 1303-1328. doi: https://doi.org/10.1007/s00382-012-1500-3

Klein, L., & Swift, C. (1977). An improved model for the dielectric constant of sea water at microwave frequencies. *IEEE Journal of Oceanic Engineering*, *2*(1), 104-111. doi: https://doi.org/10.1109/JOE.1977.1145319

Larson, S. M., Vimont, D. J., Clement, A. C., & Kirtman, B. P. (2018). How momentum coupling affects SST variance and large-scale Pacific climate variability in CESM. *Journal of Climate*, *31*(7), 2927 - 2944. doi: https://doi.org/10.1175/JCLI-D-17-0645.1

Laurindo, L. C., Mariano, A. J., & Lumpkin, R. (2017). An improved near-surface velocity climatology for the global ocean from drifter observations. *Deep Sea Research Part I: Oceanographic Research Papers*, *124*, 73-92. doi: https://doi.org/10.1016/j.dsr.2017.04.009

Laurindo, L. C., Siqueira, L., Mariano, A. J., & Kirtman, B. P. (2019). Cross-spectral analysis of the SST/10-m wind speed coupling resolved by satellite products and climate model simulations. *Climate Dynamics*, *52*(9), 5071–5098. doi: https://doi.org/10.1007/s00382-018-4434-6

Laurindo, L. C., Small, R. J., Thompson, L., Siqueira, L., Bryan, F. O., Chang, P., ... Zhang, S. (2022). Role of ocean and atmosphere variability in scale-dependent thermodynamic air-sea interactions. *Journal of Geophysical Research: Oceans*, *127*(7), e2021JC018340. doi: https://doi.org/10.1029/2021JC018340

Light, C. X., Arbic, B. K., Martin, P. E., Brodeau, L., Farrar, J. T., Griffies, S. M., ... Strobach, E. (2022). Effects of grid spacing on high-frequency precipitation variance in coupled high-resolution global ocean–atmosphere models. *Climate Dynamics*, *59*(9), 2887–2913. doi: https://doi.org/10.1007/s00382-022-06257-6

Lindstrom, E., Bryan, F., & Schmitt, R. (2015). SPURS: Salinity Processes in the Upper-ocean Regional Study — The North Atlantic Experiment. *Oceanography*, *28*(1), 14-19. doi: https://doi.org/10.5670/oceanog.2015.01

Lindstrom, E., Edson, J. B., Schanze, J. J., & Shcherbina, A. Y. (2019). SPURS-

2: Salinity Processes in the Upper-ocean Regional Study — The Eastern Equatorial Pacific Experiment. *Oceanography*, *32*(2), 15-18. doi: https://doi.org/10.5670/oceanog.2019.207

Lumpkin, R., & Johnson, G. C. (2013). Global ocean surface velocities from drifters: Mean, variance, El Niño–Southern Oscillation response, and seasonal cycle. *Journal of Geophysical Research: Oceans*, *118*(6), 2992-3006. doi: https://doi.org/10.1002/jgrc.20210

Martin, P. E., Arbic, B. K., & Hogg, A. M. (2021). Drivers of atmospheric and oceanic surface temperature variance: A frequency domain approach. *Journal of Climate*, *34*(10), 3975-3990. doi: https://doi.org/10.1175/JCLI-D-20-0557.1

Meehl, G. A., Yang, D., Arblaster, J. M., Bates, S. C., Rosenbloom, N., Neale, R., ... Danabasoglu, G. (2019). Effects of model resolution, physics, and coupling on southern hemisphere storm tracks in CESM1.3. *Geophysical Research Letters*, *46*(21), 12408-12416. doi: https://doi.org/10.1029/2019GL084057

Meissner, T., Wentz, F. J., & Le Vine, D. M. (2018). The salinity retrieval algorithms for the NASA Aquarius Version 5 and SMAP Version 3 releases. *Radio Science*, *10*(7). doi: https://doi.org/10.3390/rs10071121

Melnichenko, O. (2021). *Multi-mission L4 Optimally Interpoated Sea Surface Salinity. Ver. 1.0.* PO.DAAC, CA, USA. (Dataset accessed 2023-08-01 at https://doi.org/10.5067/SMP10-4U7CS)

Melnichenko, O., Amores, A., Maximenko, N., Hacker, P., & Potemra, J. (2017). Signature of mesoscale eddies in satellite sea surface salinity data. *Journal of Geophysical Research: Oceans*, *122*(2), 1416-1424. doi: https://doi.org/10.1002/2016JC012420

Melnichenko, O., Hacker, P., Bingham, F. M., & Lee, T. (2019). Patterns of SSS variability in the eastern tropical Pacific: Intraseasonal to interannual timescales from seven years of NASA satellite data. *Oceanography*, *32*(2), 20-29. doi: https://doi.org/10.5670/oceanog.2019.208

Melnichenko, O., Hacker., P., N. Maximenko, G. L., & Potemra, J. (2016). Optimal interpolation of Aquarius sea surface salinity. *Journal of Geophysical Research: Oceans*, *121*, 602-616. doi: https://doi.org/10.1002/2015JC011343

Melnichenko, O., Hacker, P., Potemra, J., Meissner, T., & Wentz, F. (2021). *Aquarius/SMAP sea surface salinity optimum interpolation analysis.* IPRC Technical Note. (No. 7, May 7, 2021)

Patrizio, C. R., & Thompson, D. W. J. (2021). Quantifying the role of ocean dynamics in ocean mixed-layer temperature variability. *Journal of Climate*(34), 2567-2589. doi: https://doi.org/10.1175/JCLI-D-20-0476.1

Patrizio, C. R., & Thompson, D. W. J. (2022). Understanding the role of ocean dynamics in midlatitude sea surface temperature variability using a simple stochastic climate model. *Journal of Climate*(35), 3313-3333. doi: https://doi.org/10.1175/JCLI-D-21-0184.1

Putrasahan, D. A., Kamenkovich, I., Le Hénaff, M., & Kirtman, B. P. (2017). Importance of ocean mesoscale variability for air-sea interactions in the Gulf of Mexico. *Geophysical Research Letters*, *44*, 6352-6362. doi: https://doi.org/10.1002/2017GL072884

Small, R. J., Bacmeister, J., Bailey, D., Baker, A., Bishop, S., Bryan, F., … Vertenstein, M. (2014). A new synoptic scale resolving global climate simulation using the Community Earth System Model. *Journal of Advances in Modeling Earth System*, *6*, 1065–1094. doi: https://doi.org/10.1002/2014MS000363

Small, R. J., Bryan, F. O., Bishop, S. P., Larson, S., & Tomas, R. A. (2020). What drives upper-ocean temperature variability in coupled climate models and observations. *Journal of Climate*, *33*, 577-596. doi: https://doi.org/10.1175/JCLI-D-19-0295.1

Small, R. J., Bryan, F. O., Bishop, S. P., & Tomas, R. A. (2019). Air–sea turbulent heat fluxes in climate models and observational analyses: What drives their variability? *Journal of Climate*, *32*(8), 2397 - 2421. doi: https://doi.org/10.1175/JCLI-D-18-0576.1

Smith, R., Jones, P., Briegleb, B., Bryan, F., Danabasoglu, G., Dennis, J., … Yeager, S. (2010). *The Parallel Ocean Program (POP) Reference Manual.* Los Alamos National Laboratory Tech. Rep. LAUR-10-01853. (141 pp.)

Spall, M. A. (1993). Variability of sea surface salinity in stochastically forced systems. *Climate Dynamics*, *8*(3), 151-160. doi: https://doi.org/10.1007/BF00208094

Stammer, D. (1998). On eddy characteristics, eddy transports, and mean flow properties. *Journal of Physical Oceanography*, *28*(4), 727 - 739. doi: https://doi.org/10.1175/1520-0485(1998)028⟨0727:OECETA⟩2.0.CO;2

Treguier, A. M., Deshayes, J., Lique, C., Dussin, R., & Molines, J. M. (2012). Eddy contributions to the meridional transport of salt in the North Atlantic. *Journal of Geophysical Research*, *117*(C5), C05010. doi: https://doi.org/10.1029/2012JC007927

Tulloch, R., Marshall, J., & Smith, K. S. (2009). Interpretation of the propagation of surface altimetric observations in terms of planetary waves and geostrophic turbulence. *Journal of Geophysical Research: Oceans*, *114*(C2).

doi: https://doi.org/10.1029/2008JC005055

Vinogradova, N., Lee, T., Boutin, J., Drushka, K., Fournier, S., Sabia, R., . . . Lindstrom, E. (2019). Satellite salinity observing system: Recent discoveries and the way forward. *Frontiers in Marine Science*, *6*, 243. doi: https://doi.org/10.3389/fmars.2019.00243

Wong, A. P. S., Wijffels, S. E., Riser, S. C., Pouliquen, S., Hosoda, S., Roemmich, D., . . . Park, H.-M. (2020). Argo data 1999–2019: Two million temperature-salinity profiles and subsurface velocity observations from a global array of profiling floats. *Frontiers in Marine Science*, *7*, 700. doi: https://doi.org/10.3389/fmars.2020.00700

Xie, P., Joyce, R., Wu, S., Yoo, S.-H., Yarosh, Y., Sun, F., & Lin, R. (2017). Reprocessed, bias-corrected cmorph global high-resolution precipitation estimates from 1998. *Journal of Hydrometeorology*, *18*(6). doi: https://doi.org/10.1175/JHM-D-16-0168.1

Zhang, Q., Chang, P., Yeager, S. G., Danabasoglu, G., & Zhang, S. (2022). Role of sea-surface salinity in simulating historical decadal variations of Atlantic meridional overturning circulation in a coupled climate model. *Geophysical Research Letters*, *49*(4), e2021GL096922. doi: https://doi.org/10.1029/2021GL096922

Zhang, S., Fu, H., Wu, L., Li, Y., Wang, H., Zeng, Y., . . . Guo, Y. (2020). Optimizing high-resolution community earth system model on a heterogeneous many-core supercomputing platform. *Geoscientific Model Development*, *13*(10), 4809–4829. doi: https://doi.org/10.5194/gmd-13-4809-2020

# Supporting Information for "Quantifying the contribution of ocean advection and surface flux to the upper-ocean salinity variability resolved by climate model simulations"

Lucas C. Laurindo[1], Leo Siqueira[1,2], R. Justin Small[3], LuAnne Thompson[4],

and Ben P. Kirtman[1,2,5],

[1]Rosenstiel School of Marine, Atmospheric & Earth Science, University of Miami, Miami, FL, USA.

[2]Frost Institute for Data Science and Computing, University of Miami, Miami, FL, USA.

[3]Climate and Global Dynamics Laboratory, National Center for Atmospheric Research, Boulder, Colorado, CO, USA.

[4]School of Oceanography, University of Washington, Seattle, WA, USA.

[5]Cooperative Institute for Marine and Atmospheric Studies, University of Miami, Miami, FL, USA.

## Contents of this file



---

Corresponding author: L. C. Laurindo, Rosenstiel School of Marine, Atmospheric & Earth Science, University of Miami, 4600 Rickenbacker Causeway, Miami, FL 33149-1031, USA. (llaurindo@earth.miami.edu)

## Introduction

In this Supporting Information we show global maps of contribution of the covariance between advection and surface fluxes to the total salinity variance [$\tilde{Q}_{os}$, Eq. (7) of the main manuscript] resolved by the low- and high-resolution CESM simulations (Fig. S1).

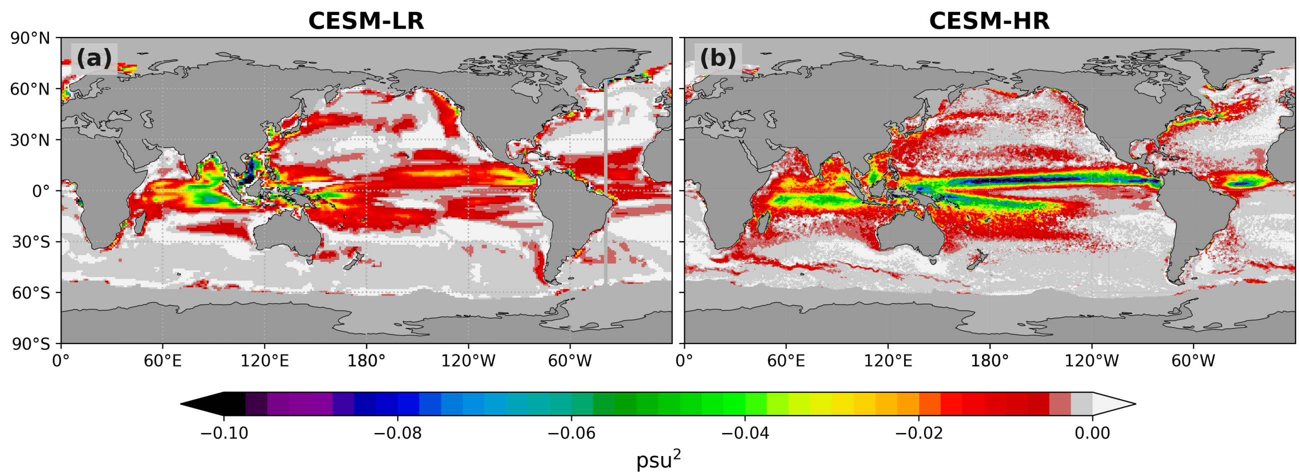


**Figure S1.** Contribution of the covariance between advection and surface freshwater fluxes to the upper-50 m salinity variance resolved by the low- and high-resolution CESM simulations.